Tsunami Hazard Assessment of Snohomish County, Washington

Project Report – Version 2

Draft of October 21, 2018

Randall J. LeVeque, Frank I. González, and Loyce M. Adams
University of Washington

Study funded by Washington State Emergency Management Division

http://depts.washington.edu/ptha/WA_EMD_Snohomish/

Contents

Notes on revised results and report

This report summarizes the final modeling results for Snohomish County submitted to the Washington State Department of Natural Resources (DNR) in October, 2018, for use in the production of maximum innundation and current speed mapping products.

This is an update of the original report (Version 1) submitted on February 27, 2018, reflecting several modifications to the computational modeling. In particular,

- In the original work, computational grids with $\Delta x = 2\Delta y$ (in degrees longitude and latitude, respectively) were used, with the finest grid resolution in the study area being 2/3 arcsecond by 1/3 arcssecond, corresponding to roughly 14 m by 10 m grid cells at the latitude of Washington. In the new study, as requested by DNR, $\Delta x = \Delta y$ was used with the finest grid resolution being 1/3 arcsecond by 1/3 arcssecond, corresponding to roughly 7 m by 10 m grid cells.

- In the original study the Seattle Fault (SF-L) event was simulated for 1–2.5 hours post-quake at most locations, with a 4 hour run only in the northern-most region. In the new study the SF-L event was run for 4 hours in all regions. Similarly, the CSZ L1 tsunami was originally simulated for 3–5.5 hours and in the new study has been simulated for at least 6 hours in all regions. This was found to have little effect on the maximum depth or current speed recorded as the maximum usually occurs over shorter times, but in a few locations this made a difference.

- The new study included simulated gauges at numerous points to record the water surface elevation (or flow depth) and the current velocities. Some of these points were specified by DNR and others chosen based on the locations of observed high current velocities in order to insure that the new run times were sufficiently long to capture the maxima properly. See Section 7.3 for some of these gauge results and more discussion.

- Some adjustments were made to the computational domain and the regions where refinement to various levels was required in order to better capture some flow features. In particular, the possible effect of flow through Deception Pass on results in the northern-most study area (region `lat_4824_4831`) was considered and determined to be insignificant.

- The most recent release of GeoClaw, Version 5.5.0, was used in the new study (together with some modifications as described in this report). The original study used GeoClaw Version 5.4.1. The new version had essentially no effect on the computed results.

The newly computed results differed from the results presented in the original study primarily due to the increase in computational resolution of the grids, but on the whole the results are very consistent with previous results, giving added confidence in the resolution used for this study and the run times chosen. The original version of this report [15] can be consulted for results to compare with those presented in this study.

We acknowledge computing time provided by the CU-CSDMS High-Performance Computing Cluster, and by the Applied Mathematics Department at the University of Washington.

1 Introduction

This report documents the results of a study supported by the Washington State Emergency Management Division of the tsunami hazard along the coast of Snohomish County. Results include inundation depths and times of arrival that will be useful to coastal communities, as well as tsunami current speeds and momentum flux. GeoClaw Version 5.5.0 was used for the modeling [4], with some modifications as described in the appendices.

Figure 1 shows the Snohomish County region and the 8 "fgmax grids" on which the results have been provided, the black rectangles in Figure 1(b). In these regions the quantities of interest have been provided as csv files on a set of points with 1/3 arcsecond spacing in longitude and 1/3 arcsecond spacing in latitude (approximately 7 m and 10 m respectively). The data format is discussed further in Section 7.1.

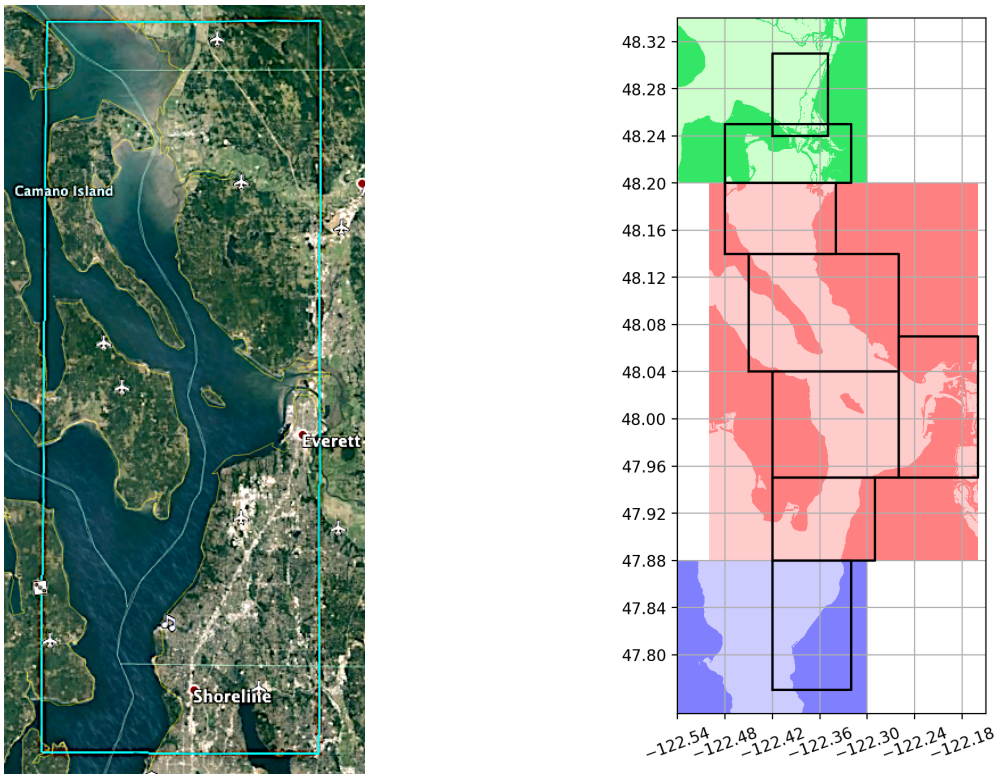

Figure 1: (a) Google Earth image. Snohomish County is delineated by the thin lines. Camano Island and Whidbey Island are in Island County, but eastern coasts of these islands are also included in the simulation results. (b) The 8 fgmax grid regions where simulation results are provided are shown as black rectangles. The green, red, and blue background show the regions where three different 1/3 arcsecond DEMs were used as topography data. In the notation introduced in Section 3, green is PT-DEM, red is Merged-DEM, blue is PS-DEM.

2 Earthquake Sources

Two earthquake sources were considered for this study: a Cascadia Subduction Zone (CSZ) megathurst event with moment magnitude Mw 9.2 (denoted CSZ-L1), and a potential Seattle Fault rupture denoted SF-L.

The CSZ-L1 event creates very large waves along the outer coast and a substantial wave that propagates into the Strait of Juan de Fuca (SJdF) and into Puget Sound, affecting parts of Snohomish County with some significant flooding, starting about 2 hours after the earthquake.

The Seattle Fault cuts across Puget Sound (through Seattle and Bainbridge Island) and can create a tsunami that affects the southern portion of Snohomish County almost immediately, and the northern portion within an hour. The larger hypothetical event SF-L considered here would cause significant inundation and high currents in parts of the County.

Other potential sources have not been considered in this study. Several other fault zones cross Puget Sound as shown in Figure 2 [28]. In particular, the South Whidbey Island Fault (SWIF) cuts through southern Snohomish County, so a tsunami generated by an earthquake on this fault could have significant effect. The SWIF was not included in the statement of work for this project due to lack of a peer-reviewed credible worst case event on this fault, although Mw 7 scenario has been used for seismic hazard studies in the past, e.g. [27].

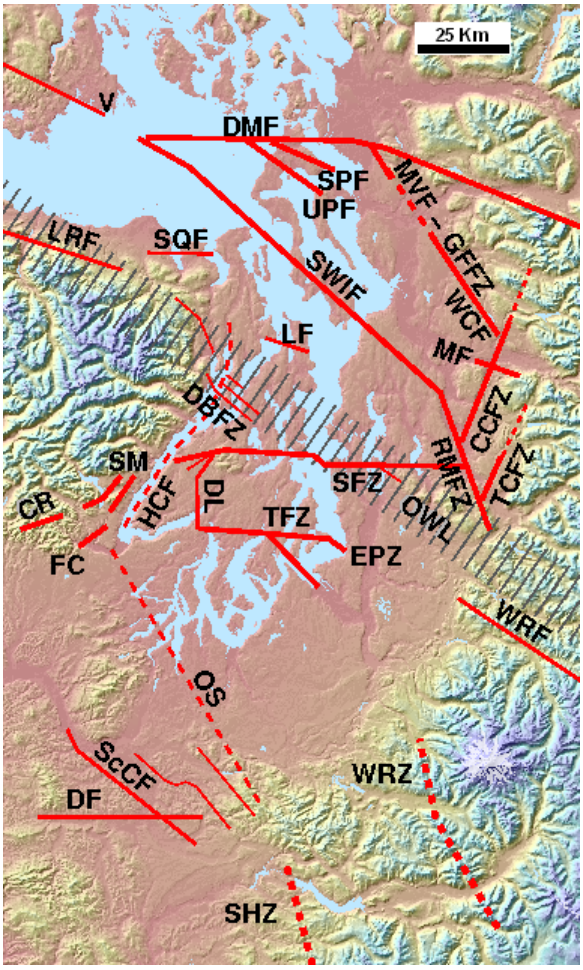

Figure 2: Puget Sound faults, including the Seattle Fault Zone (SFZ). From https://en.wikipedia.org/wiki/File:Puget_Sound_faults.png (CC-BY SA 3.0 License, attributed to J. Johnson and H. Greenberg). See [28] for discussion of the the other faults shown.

2.1 Cascadia megathrust event CSZ-L1

The probability that an earthquake of magnitude 8 or greater will occur on the Cascadia Subduction Zone (CSZ) in the next 50 years has been estimated to be 10-14% (Petersen, et. al., 2002 [20]). The last such event occurred in 1700 (Satake, et al., 2003 [22]; Atwater, et al., 2005 [1]) and future events are expected

to generate a destructive tsunami that will inundate Washington Pacific coast communities within tens of minutes after the earthquake main shock. Waves will travel through the Strait of Juan de Fuca and start arriving at Snohomish County coastlines roughly 2 hours after the earthquake.

The potential CSZ event used in this study is the L1 scenerio developed by Witter, et al. (2013) [30]; crustal deformation for the region of interest is shown in Figure 3. The L1 source is one of 15 seismic scenarios used in a hazard assessment study of Bandon, OR, based on an analysis of data spanning 10,000 years. This scenario has been adopted by Washington State as the "worst considered case" for many inundation modeling studies and subsequent evacuation map development; it is used because the standard engineering planning horizon is 2500 years and Witter, et al. (2013) [30] estimated that L1 has a mean recurrence period of approximately 3333 years, with the highest probability of occurrence of all events considered with magnitude greater than Mw 9.

The original L1 source was developed for studies on the Oregon coast and was truncated at around 48N. For past studies on the Washington coast, two different extended versions of this source have been used. One, developed by PMEL, carried the fault farther NW along Vancouver Island. The second, developed by the UW group, instead extrapolated the rupture straight northward from the line of truncation. This is less physical, but potentially directed more wave energy into the Strait. These two deformations are shown in Figure 3.

For this project DNR requested that the PMEL version of the L1 source be used to facilitate comparison with their results. We found that results obtained with the UW version were quite similar. Figure 22 shows a sample comparison of the inundation and currents near Everett when the two versions of L1 are used as sources. A comparison of these sources was also recently performed by Carrie Garrison-Laney of Washington Sea Grant, who also found that similar results were obtained in the regions she considered (Discovery Bay and Hood Canal) [8].

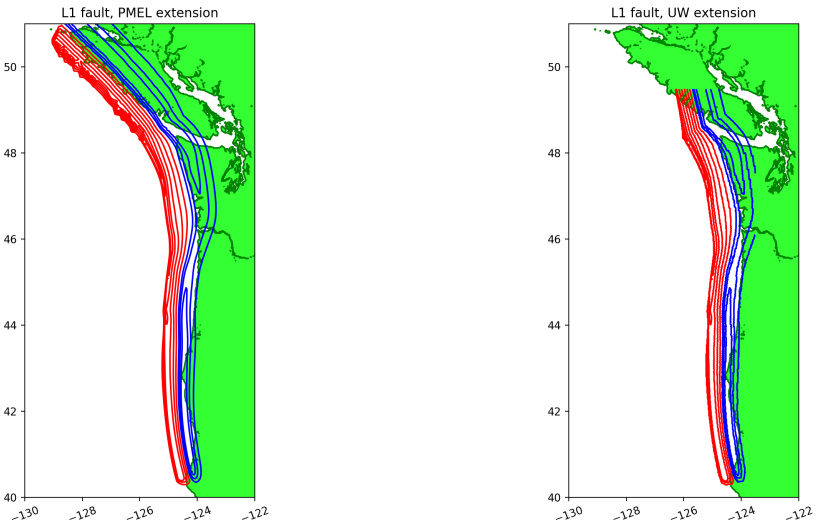

Figure 3: Surface deformation of the L1 source. The PMEL extension used on the left was used in this study, with maximum uplift 15.08 m and maximum subsidence -3.98 m. The UW extension shown on the right has been used in some past studies, with maximum uplift 15.30 m and maximum subsidence -3.99 m. In both figures, red contours show uplift (2 meter interval), blue contours show subsidence (1 meter interval).

2.2 Seattle Fault event SF-L

Figure 4 shows contours of uplift and subsidence due to a hypothetical event on the Seattle fault that we denote by SF-L. Earlier tsunami hazard studies have referred to this as a Mw 7.3 event. However, when we tried to recreate the deformation field by applying the Okada model to the subfault parameters listed in [3], we determined that the magnitude should be Mw 7.54, as discussed further in Appendix E. Regardless of the proper magnitude, we are using the deformation file provided by PMEL that has been used for the previous tsunami hazard analyses of Everett [3].

Due to uncertainty about the magnitude, we adopted the SF-L notation for this larger Seattle Fault scenario. The deformation was originally chosen to match observed uplift and subsidence at a few points around Puget Sound. Since the original specification of this deformation, many new observations have been made and improved models for the subfault geometry have also been produced. A new model for SF-L is now under development and in the future this will be used to update the results of the current study.

A smaller Seattle Fault scenario (SF-S) was also initially considered, but even more uncertainty arose over the proper specification of fault slip for this event, and so this has not been used in the present study. Appendix E contains some discussion of difficulties with this scenario, for future reference. Some preliminary simulations with different versions of SF-S showed very little inundation and few regions of high currents in Snohomish County (see Figure 28 for one sample result). A new SF-S source is also currently under development that may be used in future tsunami hazard assessment.

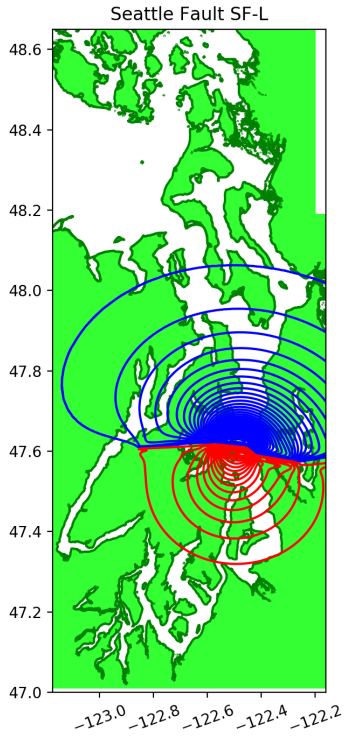

Figure 4: Surface deformation for Seattle Faulte event SF-L. The blue contours show subsidence at levels -0.05, -0.1, ... meters, with maximum subsidence -1.78m. The red contours show uplift at levels 0.5, 1, 1.5, ... meters, with maximum uplift 8.37m.

3 Topography and Bathymetry

3.1 1/3 Arc-second DEMs

Output from the model was requested at grid points spaced 1/3" in longitude and 1/3" in latitude, with the points aligned with cell centers of the 1/3" DEM files that are available for the Puget Sound region. (Note that 1/3" in latitude is approximately 10.3 m. At this latitude, 1/3" in longitude is approximately 6.9 m).

GeoClaw uses finite volume methods with adaptive mesh refinement, and the finest grid resolution near regions of interest was set to the desired resolution of 1/3" by 1/3".

Unfortunately there is no single DEM that provides 1/3" topography and bathymetry for all of Snohomish County. The Puget Sound 1/3 Arc-second MHW Coastal Digital Elevation Model [17] (referred to below as PS-DEM) only extends up to 48.19N, while the Port Townsend 1/3 Arc-second MHW Coastal Digital Elevation Model [16] (referred to below as PT-DEM) only extends as far south as 47.91N. Moreover, we found that these two DEMs did not agree well in the region where they overlap, with offshore values differing by nearly 1 m (while onshore values often agreed). See Section B for further discussion and an illustration. These DEMs are both supposed to be referenced to MHW, but since the tidal range varies considerably over the Sound, they are presumably referenced to different values of MHW relative to the WGS84 geoid.

NCEI provided a custom merged DEM extending from 47.88N to 48.2N that smoothly matches the PS-DEM to the south and the PT-DEM to the north, and that uses the best available data. This will be referred to as Merged-DEM, and was used in this latitude range rather than PS-DEM or PT-DEM. Figure 1(b) shows the regions covered by the three 1/3" DEMs (green is PT-DEM, red is Merged-DEM, blue is PS-DEM).

Figure 5 shows a blowup of Figure 1(b) for the region just south of Stanwood, at the north end of Port Susan (the bay between Camano Island and the mainland), in the Stillaguamish River delta. Lighter shades indicate topography below MHW, darker shades indicate regions above MHW. Note the signficant regions of farmland that lie below MHW and that are separated from the bay by narrow dikes. Matching the topography correctly is critical in this region.

Properly capturing tsunami inundation in the regions of these dikes is also difficult to do properly. This problem and the limitations of the modeling results in these regions are discussed further in Section 4.

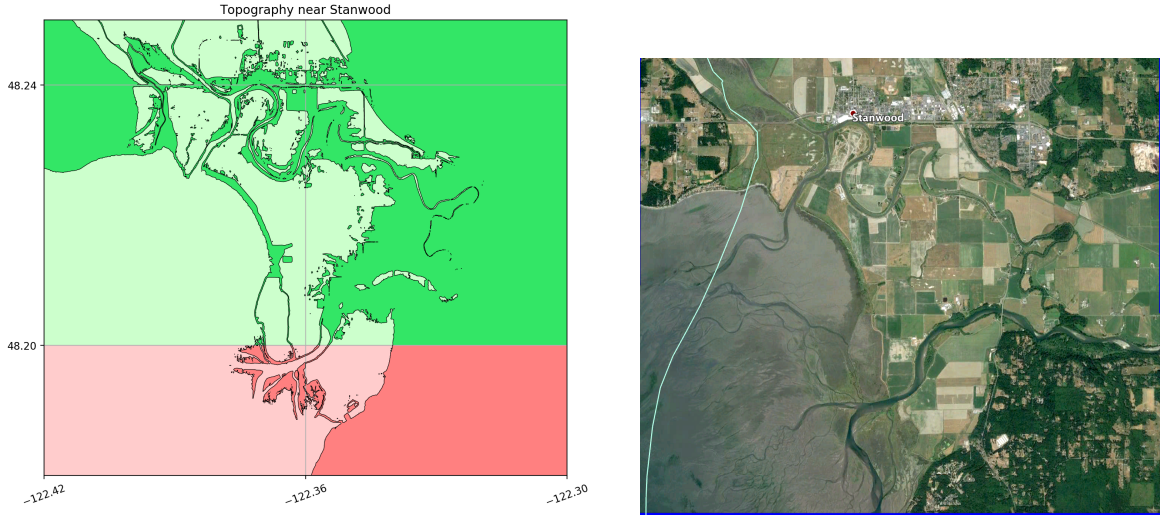

Figure 5: (a) Blow up of Figure 1(b) for the region just south of Stanwood, showing land in the Stillaguamish River delta that is below MHW (lighter shades) and protected by dikes. (b) Google Earth image of the same region.

3.2 Coarser DEMs

The 1/3" PT-DEM and PS-DEM discussed above were also coarsened to obtain 2" DEMs for a larger region. These DEMs are more efficient to use in GeoClaw on coarser grid levels where all the details of the 1/3" DEMs are not required. In addition to these two DEMs, for simulations of the CSZ L1 event, a 2" DEM of the Strait of Juan de Fuca was used that was obtained by coarsening the 1/3" Strait of Juan de Fuca DEM [18]. Outside of the Strait and sound, etopo 1-minute topography for the Pacific Ocean and outer coasts was used.

4 Modeling dikes and dry land below MHW

As noted above, much of the farmland in the Stillaguamish River Delta just south of Stanwood is below MHW and kept dry by a network of dikes. The same is true of the region north of Stanwood, and dikes run all along the coast from Stanwood to the northern border of Snohomish County and beyond, where Fir Island and much of the Skagit River Valley are below MHW. There are also many areas around Everett that are below MHW and protected by dikes or roadways.

There are several fundamental difficulties in properly modeling tsunami inundation in these regions. If the computational grid is not sufficiently fine, then the thin dikes may not be properly captured on the grid, resulting in a gap in the dike that water will naturally flow through, even if the land behind the dike is initialized as dry in the computation. Some of the dikes shown in Figure 5 are only a few grid cells wide (or less) on the 1/3" DEM. Since the finite volume method uses topography values in each computational cell that come from cell-averaging a piecewise bilinear function defined by the DEM, additional gaps in the dikes appear at some locations.

Another problem is with the initialization. The standard approach to initializing the fluid depth in each grid cell at the start of the computation is to set $h = 0$ in any cell for which the topography value satisfies $B > 0$, and to set the depth $h = -B > 0$ in any cell for which $B < 0$, so that the water surface is at $\eta = h + B = 0$ in these cells. Since $B = 0$ corresponds to MHW, this fills the Sound with water that is at MHW everywhere before it is disturbed by the earthquake deformation.

The problem is that a grid cell that corresponds to dry land behind a dike may have $B < 0$ and yet we should set $h = 0$ to initialize this to the dry state. For complicated topography such as that shown in Figure 5, it is nontrivial to determine which points are wet and which should be dry. A new procedure to accomplish this has been partially developed as part of this project, but it does not yet work robustly in connection with the adaptive mesh refinement algorithms in GeoClaw. It also naturally fails if there is a gap in the finite volume representation of the dike. Some additional discussion of this potential improvement to GeoClaw is included in Appendix C.

An additional challenge when trying to predict realistic tsunami inundation is that it is not known which of the levies might fail due to seismic shaking, and/or be breached by the tsunami, with erosion lowering the height and allowing much more flood water to enter than would be predicted from overtopping of a fixed dike at the original height. GeoClaw, like most other current tsunami models, does not model erosion and changes in the topography, and at any rate the potential seismic damage is not accounted for.

Because of these difficulties, in consultation with DNR it was determined that the best approach currently is to use the traditional initialization of GeoClaw, which floods all regions behind dikes with water up to the MHW level before the simulation starts. The results might then be viewed as a "worst case" in which all dikes are breached. Results should be interpreted with this in mind.

See Figure 9 for an illustration of the regions near Stanwood. All of the blue points are below MHW, including extensive regions behind dikes. Figure 7 shows the region near Everett, where there are also extensive regions east of interstate I-5 that are below MHW. These regions extend east of longitude -122.16, the limit of the 1/3" DEM. However, in none of the simulations did inundation reach these regions and so additional topography data was not needed.

5 Modeling uncertainties and limitations

The simulations of tsunami generation, propagation and inundation were conducted with the GeoClaw model. This model solves the nonlinear shallow water equations, has undergone extensive verification and validation (e.g. [2, 14], and has been accepted as a validated model by the U.S. National Tsunami Hazard Mitigation Program (NTHMP) after conducting multiple benchmark tests as part of an NTHMP benchmarking workshop [9].

Several important geophysical parameters must be set in the GeoClaw software, and some physical processes are not included in these simulations, which use the two-dimensional shallow water equations. These are discussed below along with their potential effect on the modeling results.

5.1 Tide stage and sea level rise

The simulations were conducted with the background sea level set to MHW. This value is conservative, in the sense that the severity of inundation will generally increase with a higher background sea level. Larger tide levels do occasionally occur, but the assumption of MHW is standard practice in studies of this type. Potential sea level rise over the coming decades was not taken into account in this modeling.

5.2 Subsidence

The Seattle Fault event SF-L causes some subsidence of the study area: the negative deformation contours shown in Figure 4 extend into Snohomish County. This subsidence is accounted for in the GeoClaw modeling. The initial DEM provided for the region is modified by the deformation by the earthquake deformation. See Appendix A.3 for more details.

5.3 Structures

Buildings were not included in the simulations, the topographic DEMs provided for this study are "bare earth". The presence of structures will alter tsunami flow patterns and generally impede inland flow. To some extent the lack of structures in the model is therefore a conservative feature, in that their inclusion would generally reduce inland penetration of the tsunami wave. However, as in the case of the friction coefficient, impeding the flow can also result in deeper flow in some areas. It can also lead to higher fluid velocities, particularly in regions where the flow is channelized, such as when flowing up streets that are bounded by buildings.

5.4 Bottom friction

Mannings coefficient of friction was set to 0.025, a standard value used in tsunami modeling that corresponds to gravelly earth. This choice of 0.025 is conservative in some sense, because the presence of trees, structures and vegetation to the west of the Long Beach Elementary School campus would justify the use of a larger value, which might tend to reduce the inland flow. On the other hand, larger friction values can lead to deeper flow in some areas, since the water may pile up more as it advances more slowly across the topography. A sensitivity study using other friction values has not been performed.

5.5 Tsunami modification of bathymetry and topography

Severe scouring and deposition are known to occur during a tsunami, undermining structures and altering the flow pattern of the tsunami itself. Again, this movement of material requires an expenditure of tsunami energy that tends to reduce the inland extent of inundation. On the other hand, if natural berms or ridges along the coastline (or man-made levies or dikes) are eroded by the tsunami, then some areas can experience much more extensive flooding. There is no erosion or deposition included in the simulations presented here.

6 Study regions

The coast of Snohomish County was subdivided into 8 rectangular regions, as shown in Figure 1(b). These will be referred to as *fgmax regions* since these are regions on which a fixed grid is defined (independent of adaptive refinement) on which the maximum of each quantity of interest is monitored during the course of the simulation. The quantities monitored are the flow depth, flow speed, and momentum flux, along with the time at which the maximum is attained and the first arrival time of significant waves at each grid point. For each earthquake event considered, 8 different GeoClaw runs were performed, one focusing on each of these regions.

In the revised work a 9th region has been added that overlaps two of the previous regions, due to some discrepancies observed in the results from near the boundary between two of the original regions. See Section 6.1 for discussion of this region.

The fgmax points lie on a grid with spacing 1/3" by 1/3" that is aligned with the DEM grids. However, an improvement to GeoClaw developed for this project allows selecting only the grid points in each region for which the topography elevation is below some limit, here taken to be 40 m. We assume that points with greater elevation will not be inundated with any of the events considered — a good assumption since inundation depths were a few meters at most. The elevation 40 m was set higher than necessary in order to insure that a buffer of dry points exists around the inundation region to facilitate interpreting the results (at the request of DNR).

If only onshore inundation and near shore currents need to be modeled, then one could also set a lower threshold, e.g. −40 m, and only select grid points where the bathymetry elevation is above this value. For this project we included all water points in order to model currents everywhere.

Region label	Landmark	West	East	South	North	Count	Figures
lat_4824_4831	Stanwood north	-122.42	-122.35	48.24	48.31	555,221	6, 11
lat_4820_4825	Stanwood south	-122.48	-122.32	48.20	48.25	810,674	6, 12
lat_4814_4820	Port Susan	-122.48	-122.34	48.14	48.20	832,005	7, 13
lat_4804_4814	Tulalip Bay	-122.45	-122.26	48.04	48.14	1,407,583	7, 14
lat_4795_4804	Hat Island	-122.42	-122.26	47.95	48.04	1,214,471	8, 15
lat_4795_4807	Everett	-122.26	-122.16	47.95	48.07	1,158,634	8, 16
lat_4788_4795	Possession Sound	-122.42	-122.29	47.88	47.95	693,794	9, 17
lat_4777_4788	Edmonds	-122.42	-122.32	47.77	47.88	778,890	9, 18
lat_4800_4808	Overlap	-122.42	-122.26	48.00	48.08	1,214,471	10, 19
						8,599,835	Total

Table 1: The eight fgmax regions, listed from north to south. The fgmax points are aligned with the DEM in the regions specified, with 1/3" spacing in longitude and 1/3" in latitude. Only grid points for which the topography elevation is less than 40 m were used, and the column labeled "Count" gives the number of fgmax points in each region. See Figures 6–10 for plots of the fgmax max points colored by elevation, and Figures 11– 19 for plots of the simulation results.

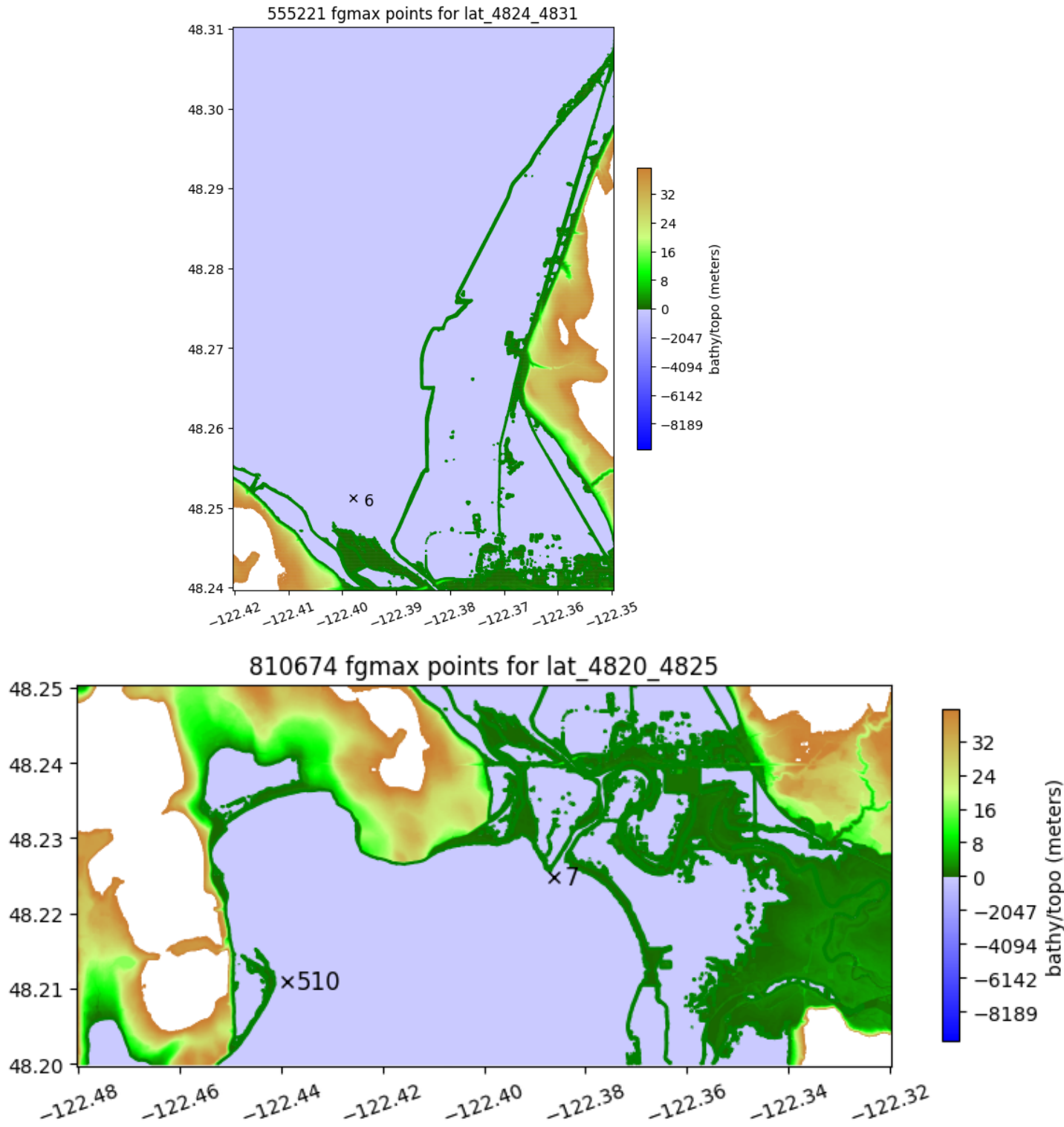

Figure 6: The topography elevation at the fgmax points for regions north of Stanwood (top) and south of Stanwood (bottom). Locations of synthetic gauges in this region are also shown at × points. See Section 7.3.

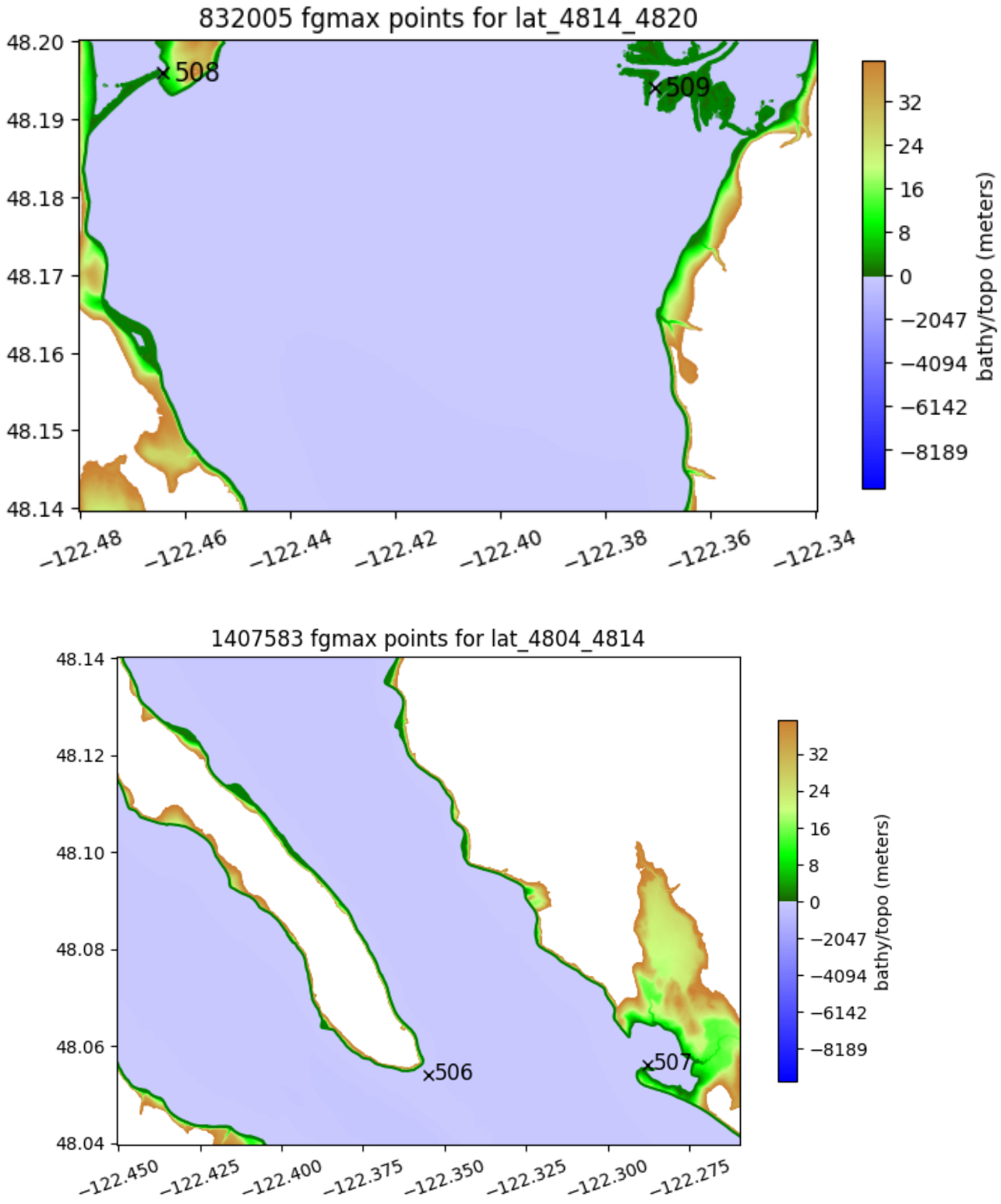

Figure 7: The topography elevation at the fgmax points for regions near central Port Susan (top) and Tulalip Bay (bottom). Locations of synthetic gauges in this region are also shown at × points. See Section 7.3.

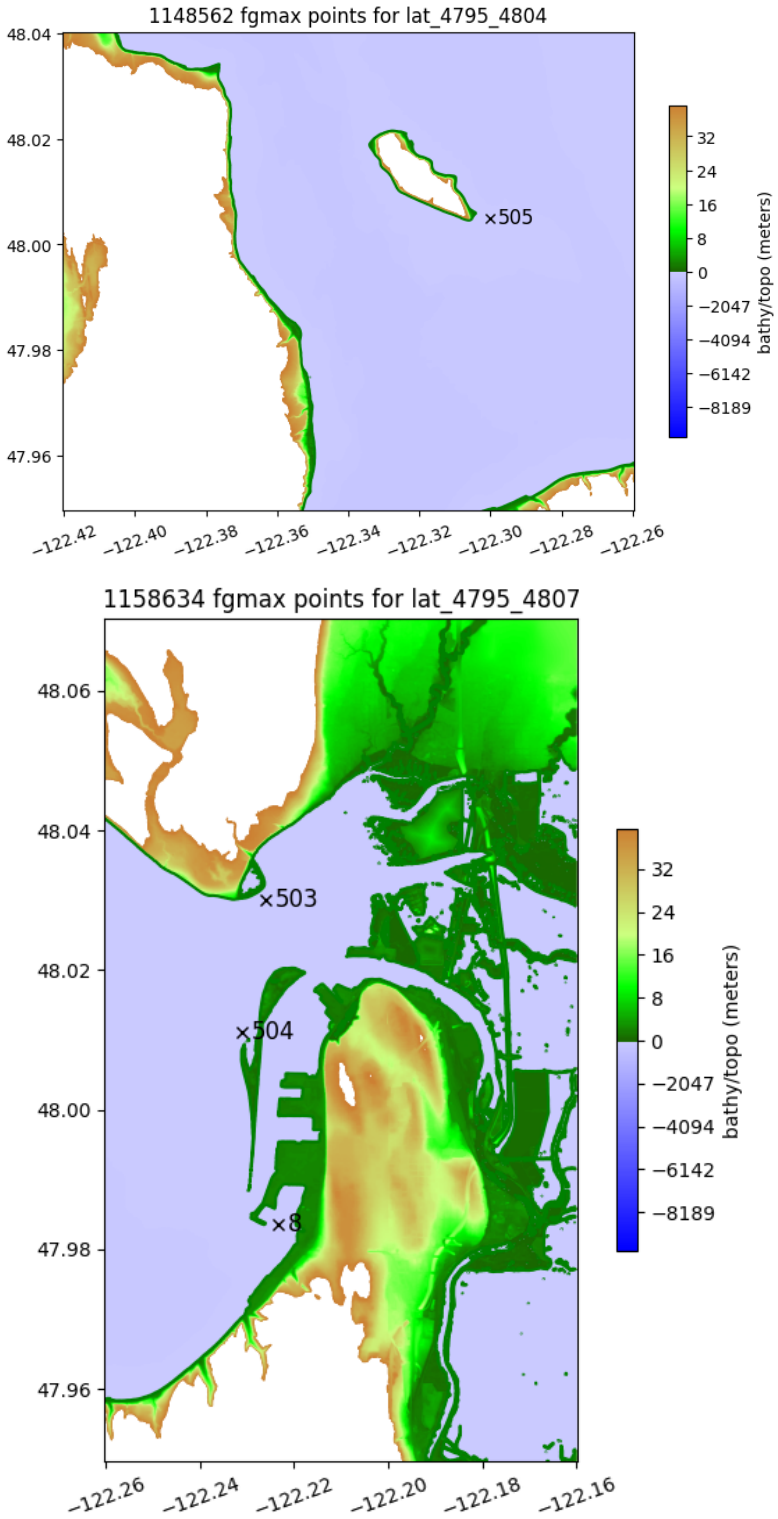

Figure 8: The topography elevation at the fgmax points for regions near Hat (Gedney) Island (top) and Everett (bottom). Locations of synthetic gauges in this region are also shown at × points. See Section 7.3.

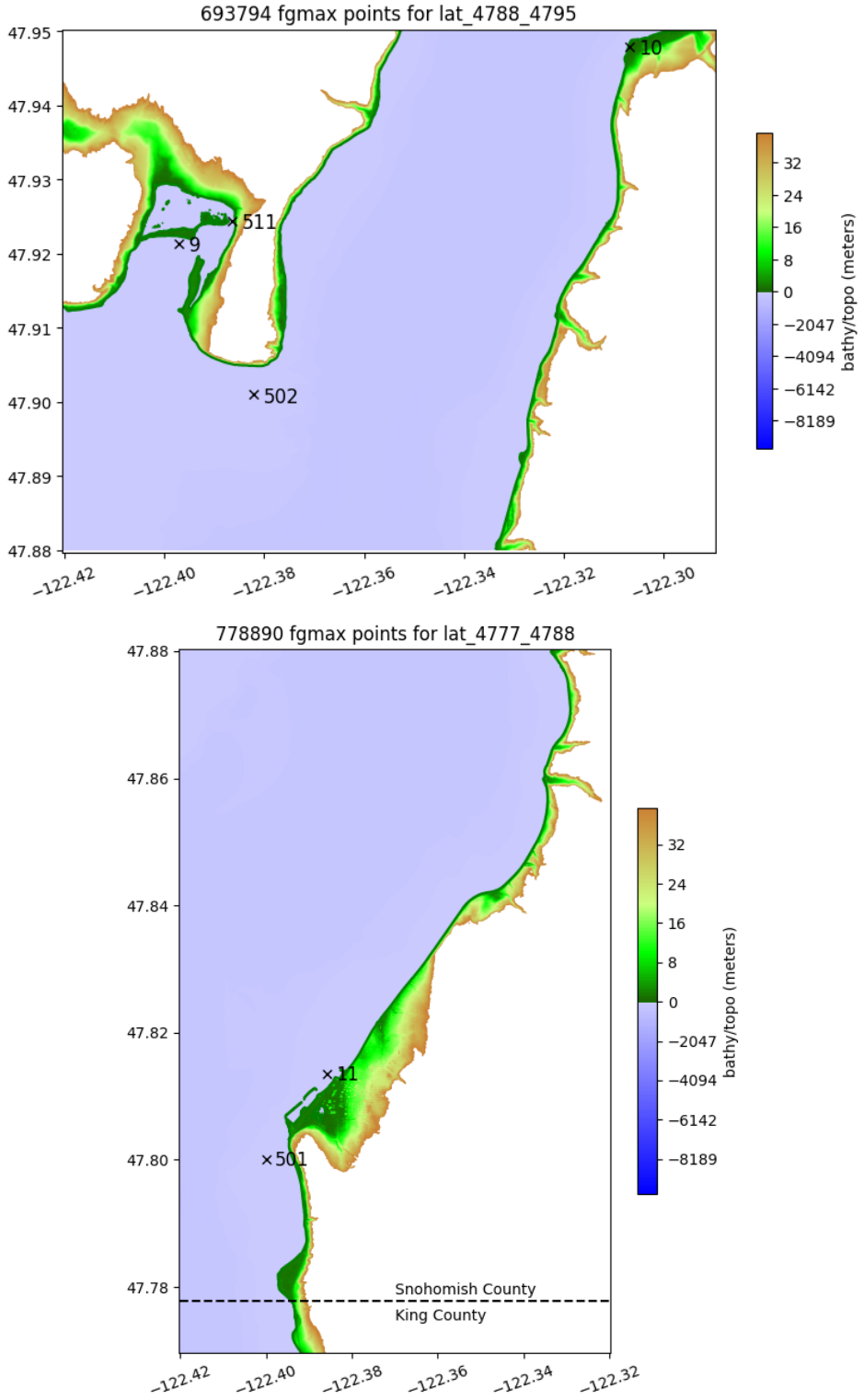

Figure 9: The topography elevation at the fgmax points for regions near Possession Sound (top) and Edmonds (bottom). Locations of synthetic gauges in this region are also shown at × points. See Section 7.3.

6.1 Overlap region

In the revised study a new region was introduced from latitude 48.00 to 48.08 denoted by `lat_4800_4808` that overlaps two of the original regions `lat_4804_4814` (Tulalip Bay) and `lat_4795_4804` (Hat Island). This region was used to obtain better results near the boundaries of the two original regions, where the maximum speed plots revealed a minor inconsistency in the original results.

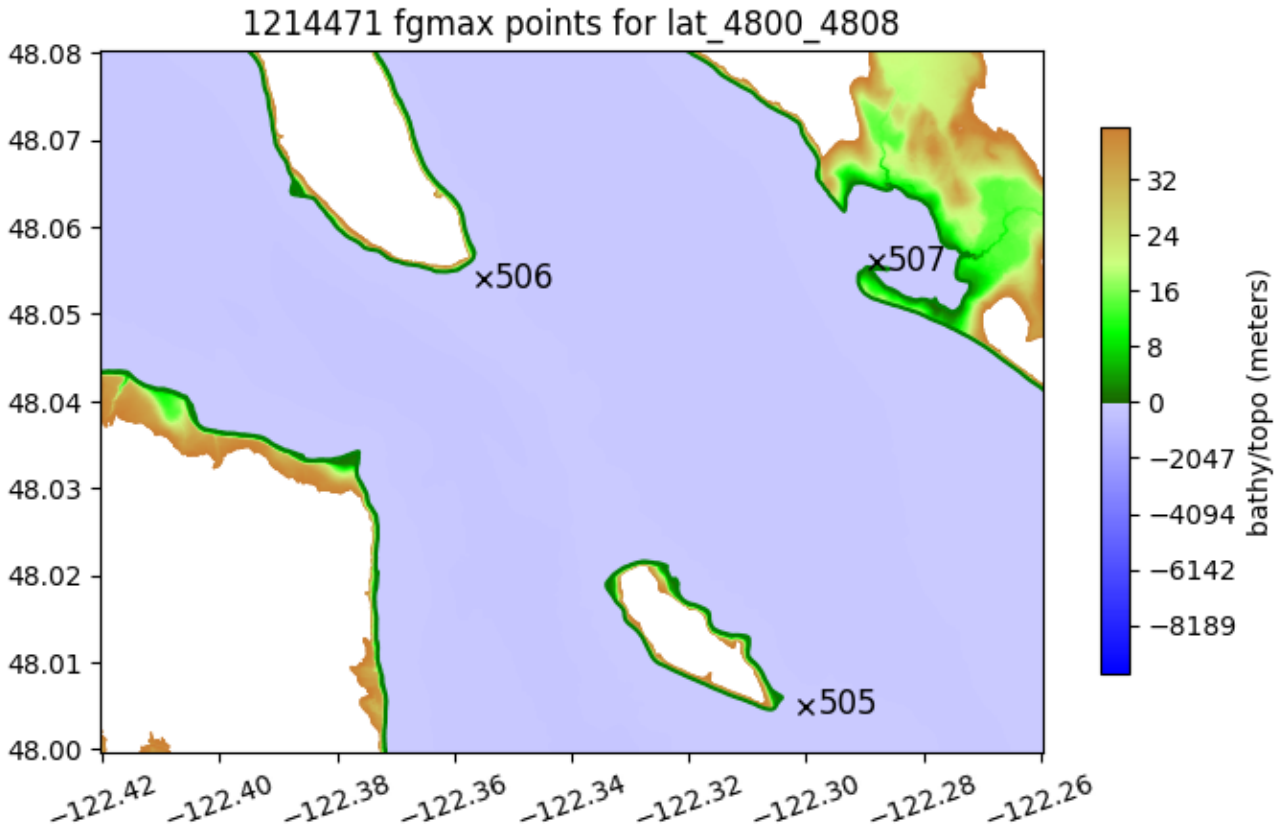

Figure 10: The topography elevation at the fgmax points for the overlap region between Tulalip Bay and Hat Island. Locations of synthetic gauges in this region are also shown at × points. See Section 7.3.

7 Results

7.1 Data format

For each earthquake source, output data is provided in a set of csv files, one for each of the regions listed in Table 1 and shown in Figures 6–10. There are nine files for each source and two sources, so a total of 18 csv files are provided with results.

For example, the southernmost region has two associated files:

- `lat_4777_4788_L1pmel_fgmax.csv` results using the CSZ L1 source (as provided by PMEL),
- `lat_4777_4788_SFL_fgmax.csv` results using the larger Seattle Fault event.

Each file has a one-line header followed by a line of data for each fgmax point in the region.
The columns are:

1. longitude (degrees)
2. latitude (degrees)
3. topography elevation z from the DEM (meters)
4. topography value B from GeoClaw for the grid cell (m)
5. subsidence dz interpolated from deformation file (m)
6. maximum fluid depth h (m)
7. maximum fluid velocity (m/s)
8. maximum momentum flux (m^3/s^2)
9. arrival time (seconds)

The fgmax points are exactly aligned with the 1/3" DEM, although sampled at 1/3" in longitude. The finest level computational finite volume grid is also aligned so that cell centers are exactly at the fgmax points, and z in column 3 is the value from the DEM at this point. However, the topography value B used in a grid cell in GeoClaw is obtained by integrating a piecewise bilinear function that interpolates the 1/3" DEM, and so B does not exactly equal z.

Format of gauge output csv files.

The gauge time series is recorded in csv files with columns

1. time (seconds post-quake),
2. topography value B from GeoClaw at gauge location (m),
3. depth of water at gauge in simulation (m),
4. E/W velocity u at gauge (m/s),
5. N/S velocity v at gauge (m/s).

7.2 Sample results

We have not attempted to produce high quality graphics of the results, since Washington State DNR is taking our raw data and producing the maps that will be published elsewhere. However, we provide some plots to give an indication of the sort of flooding and flow speeds observed, and for future reference if the simulations are re-run at a later date.

Some sample results are shown in Figures 11 through 19. Note that some points shown as light blue in the speed plots have elevation lower than MHW, but are behind dikes in regions that do not necessarily inundate, as discussed in Section 4. In the maximum flow depth plots (the left plot in each figure), points are masked out if the original topography elevation is below MHW (even if it is an onshore point that might or might not have flooded). Points with elevation greater than 40 m are also masked out (in both depth and speed plots) since no fgmax points were located in these regions. Points shown in green in the plots below are fgmax points that were originally onshore and that did not flood.

The CSZ L1 results are very similar regardless of whether the source extension developed by PMEL or by UW was used (see Section 2.1). The inundation and flow speed patterns are quite similar to those observed with SF-L, the larger Seattle Fault event.

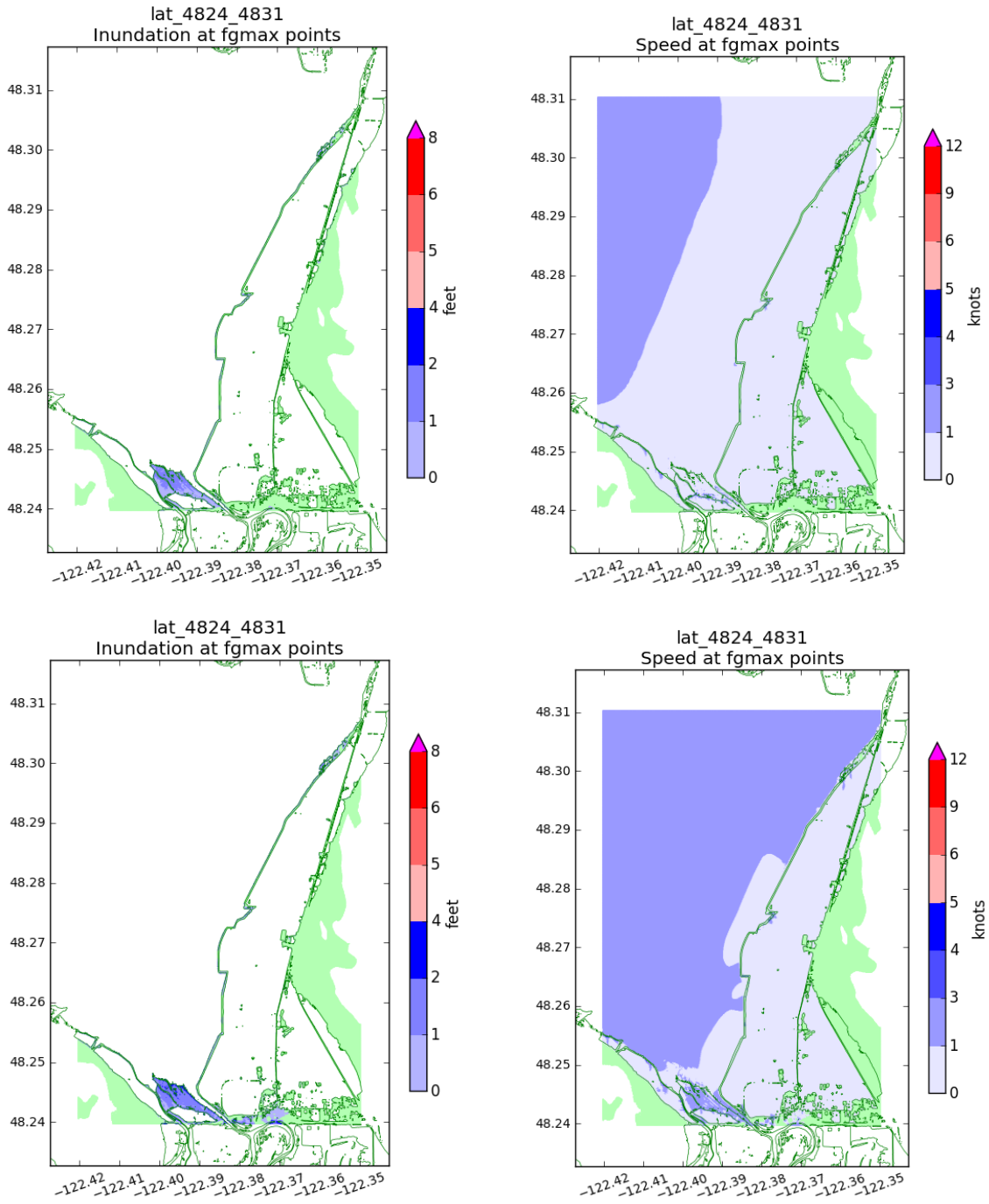

Figure 11: Sample results for the Region `lat_4824_4831`. Top: SF-L, Bottom: CSZ-L1, Left: Depth, Right: Speed.

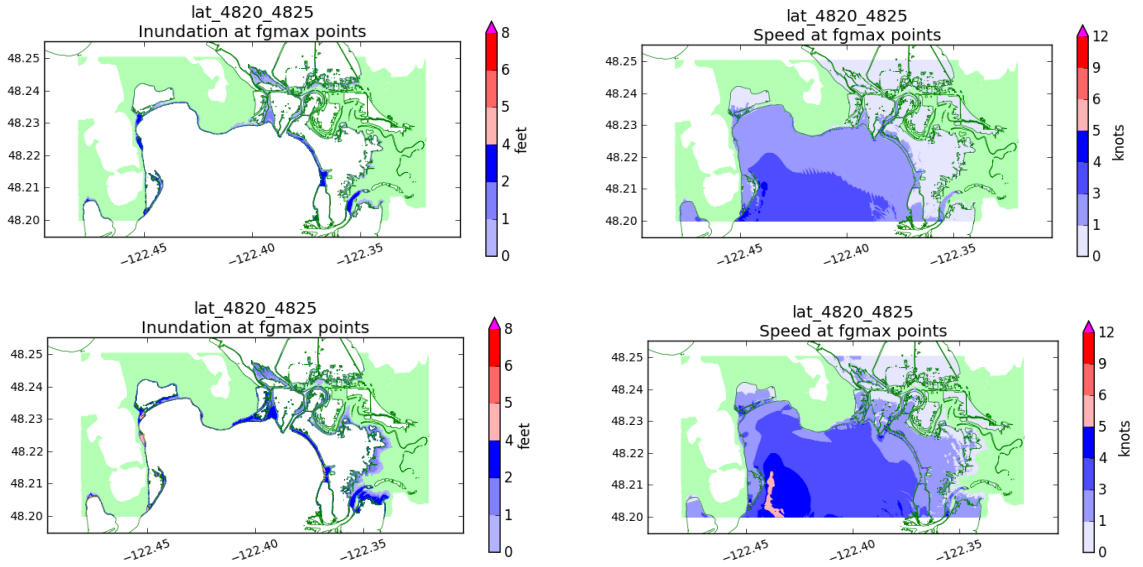

Figure 12: Sample results for the Region `lat_4820_4825`. Top: SF-L, Bottom: CSZ-L1, Left: Depth, Right: Speed.

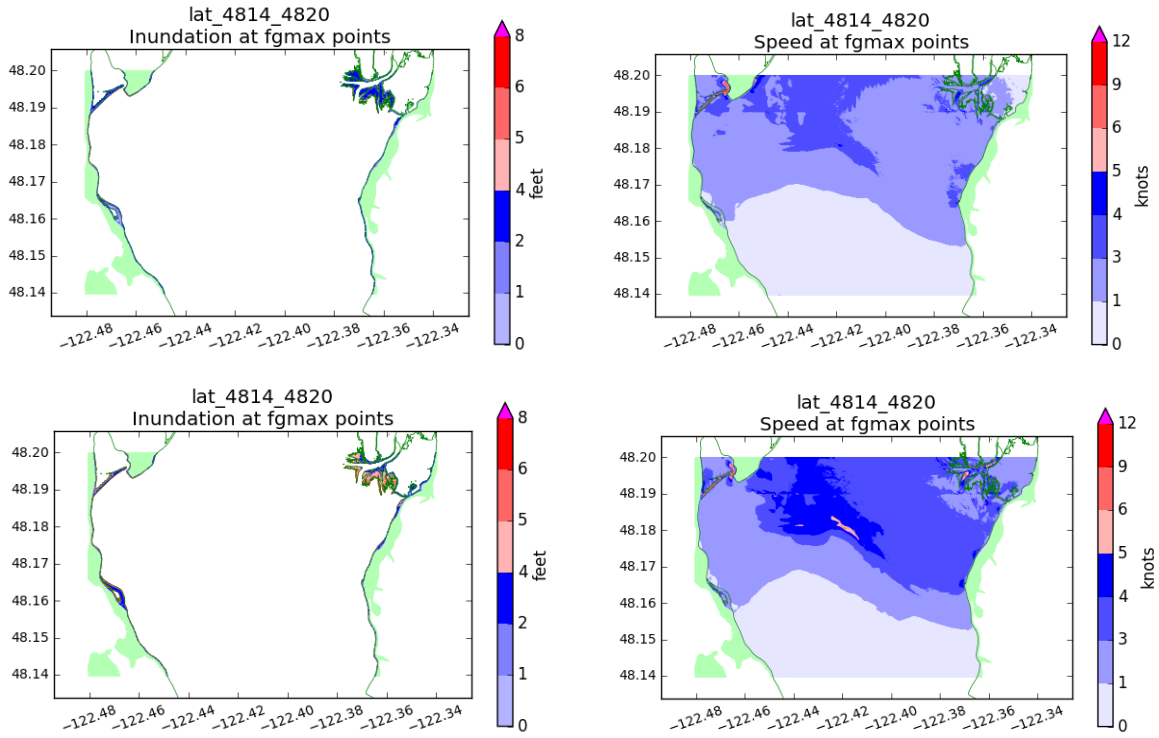

Figure 13: Sample results for the Region `lat_4814_4820`. Top: SF-L, Bottom: CSZ-L1, Left: Depth, Right: Speed.

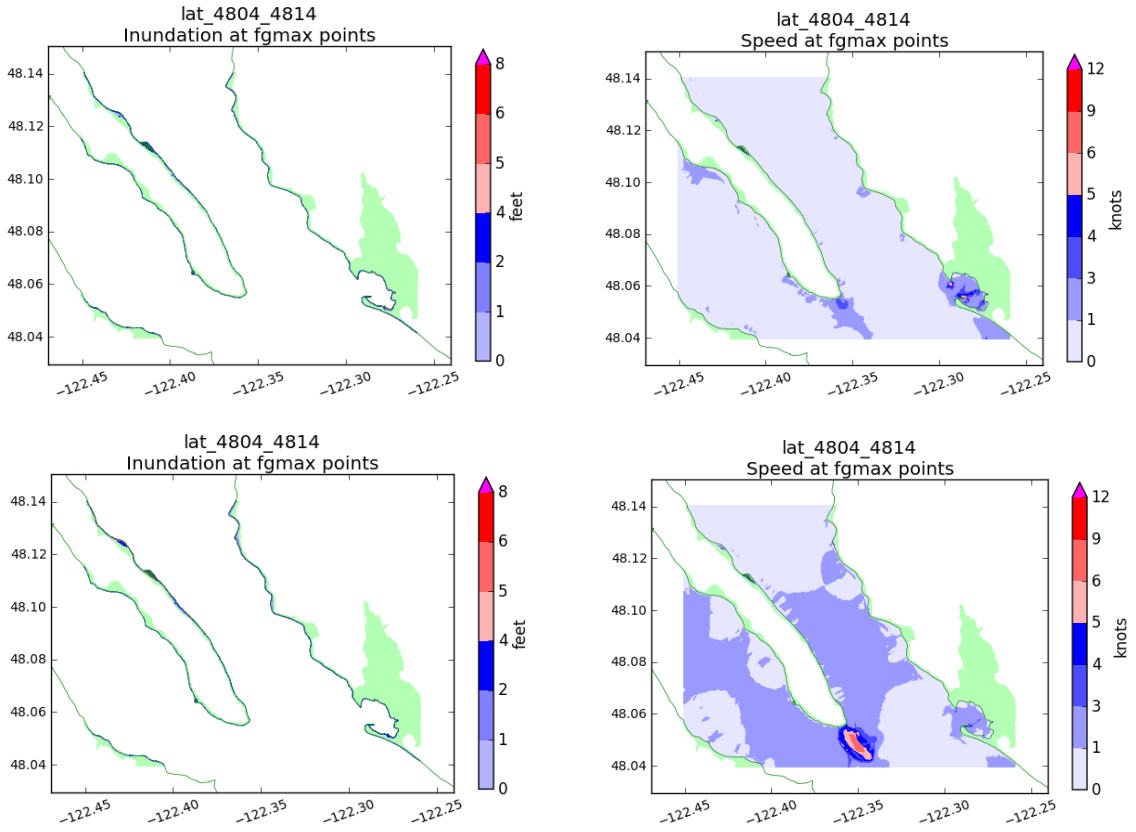

Figure 14: Sample results for the Region `lat_4804_4814`. Top: SF-L, Bottom: CSZ-L1, Left: Depth, Right: Speed.

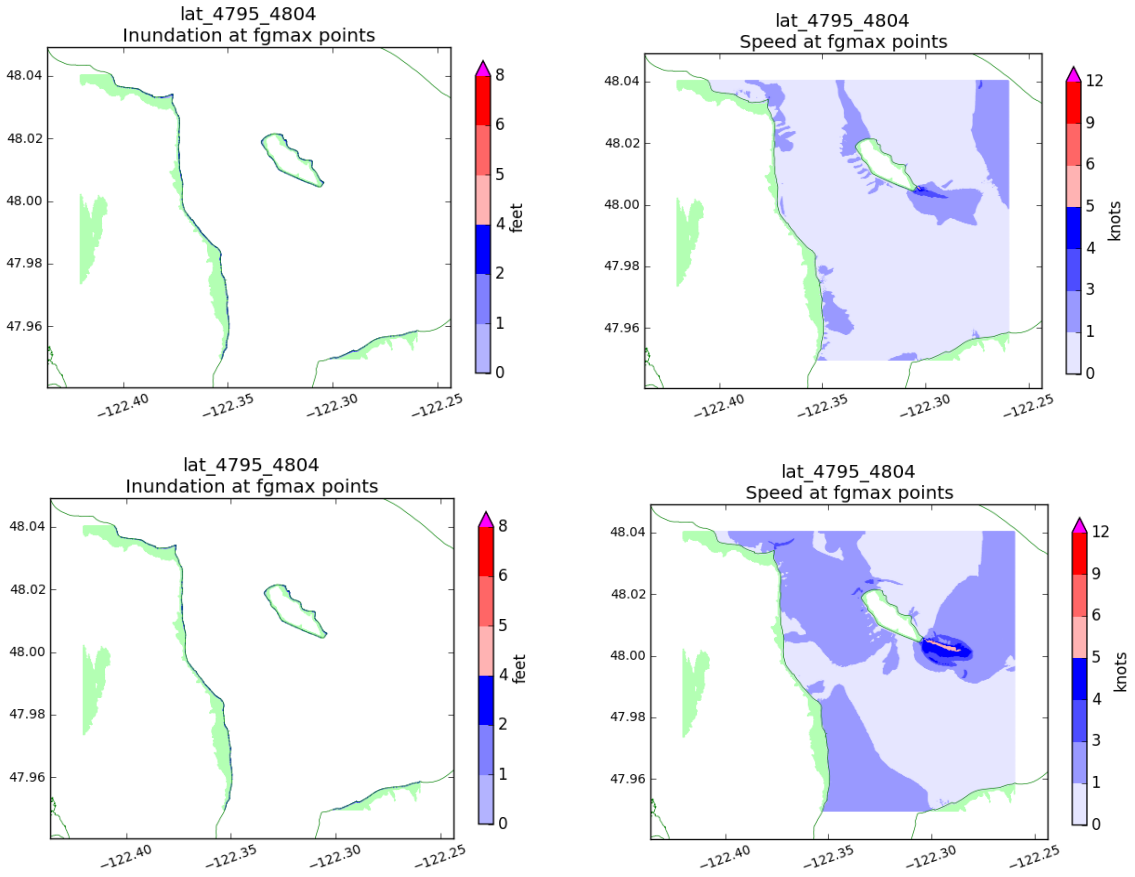

Figure 15: Sample results for the Region `lat_4795_4804`. Top: SF-L, Bottom: CSZ-L1, Left: Depth, Right: Speed.

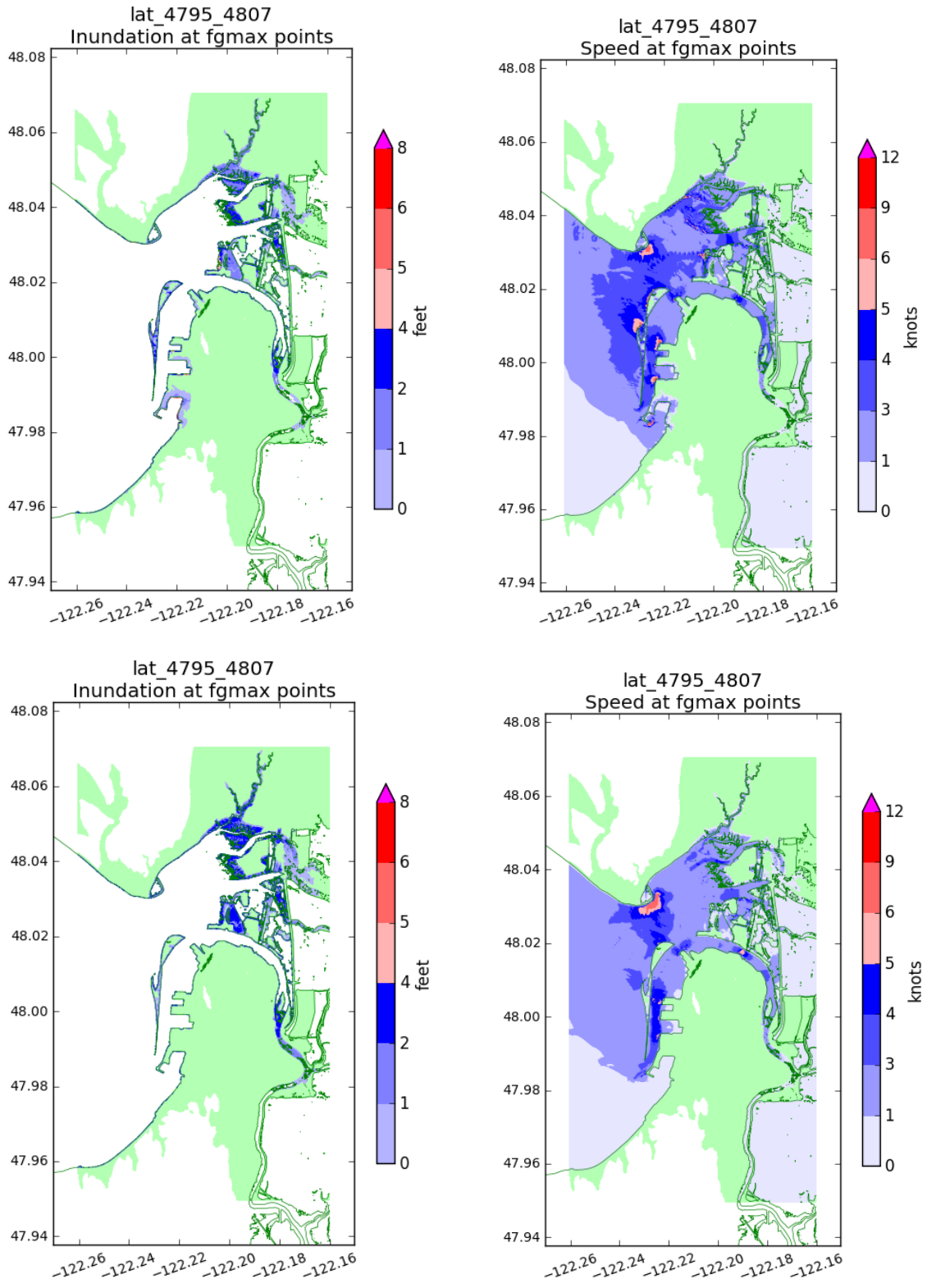

Figure 16: Sample results for the Region `lat_4795_4807`. Top: SF-L, Bottom: CSZ-L1, Left: Depth, Right: Speed.

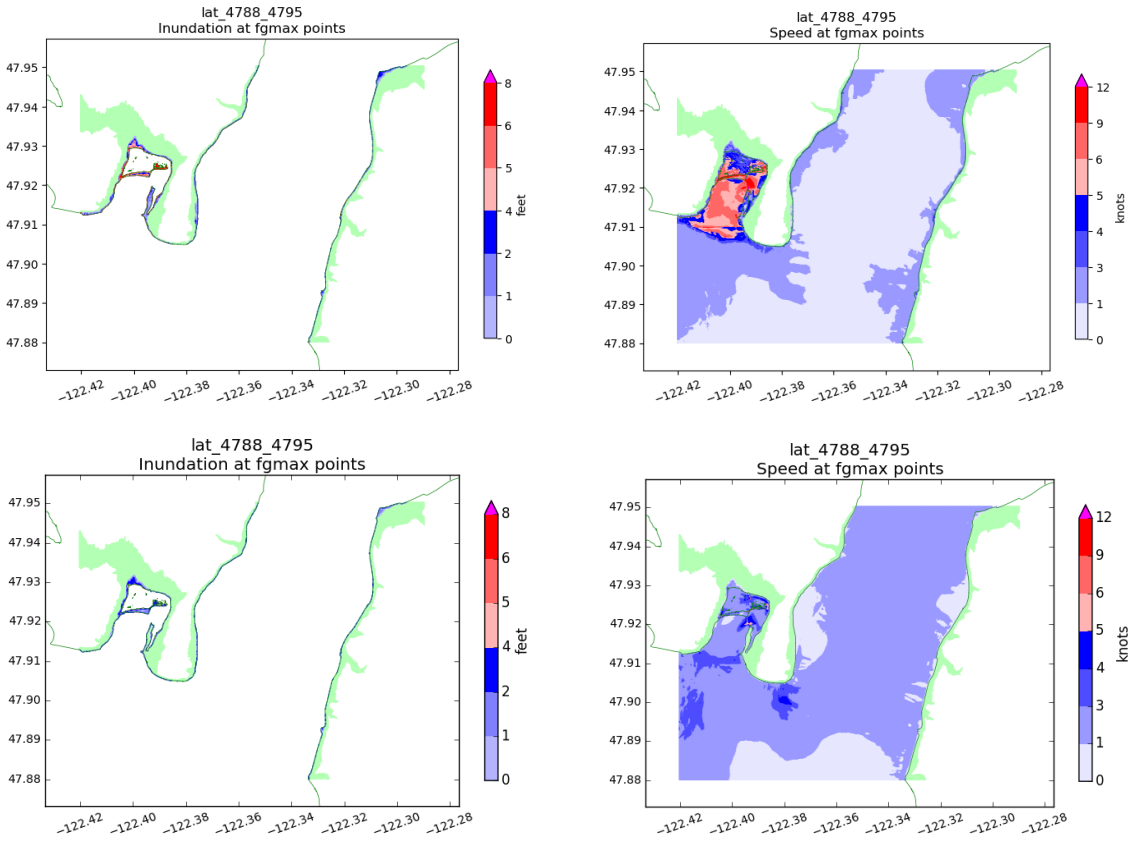

Figure 17: Sample results for the Region `lat_4788_4795`. Top: SF-L, Bottom: CSZ-L1, Left: Depth, Right: Speed.

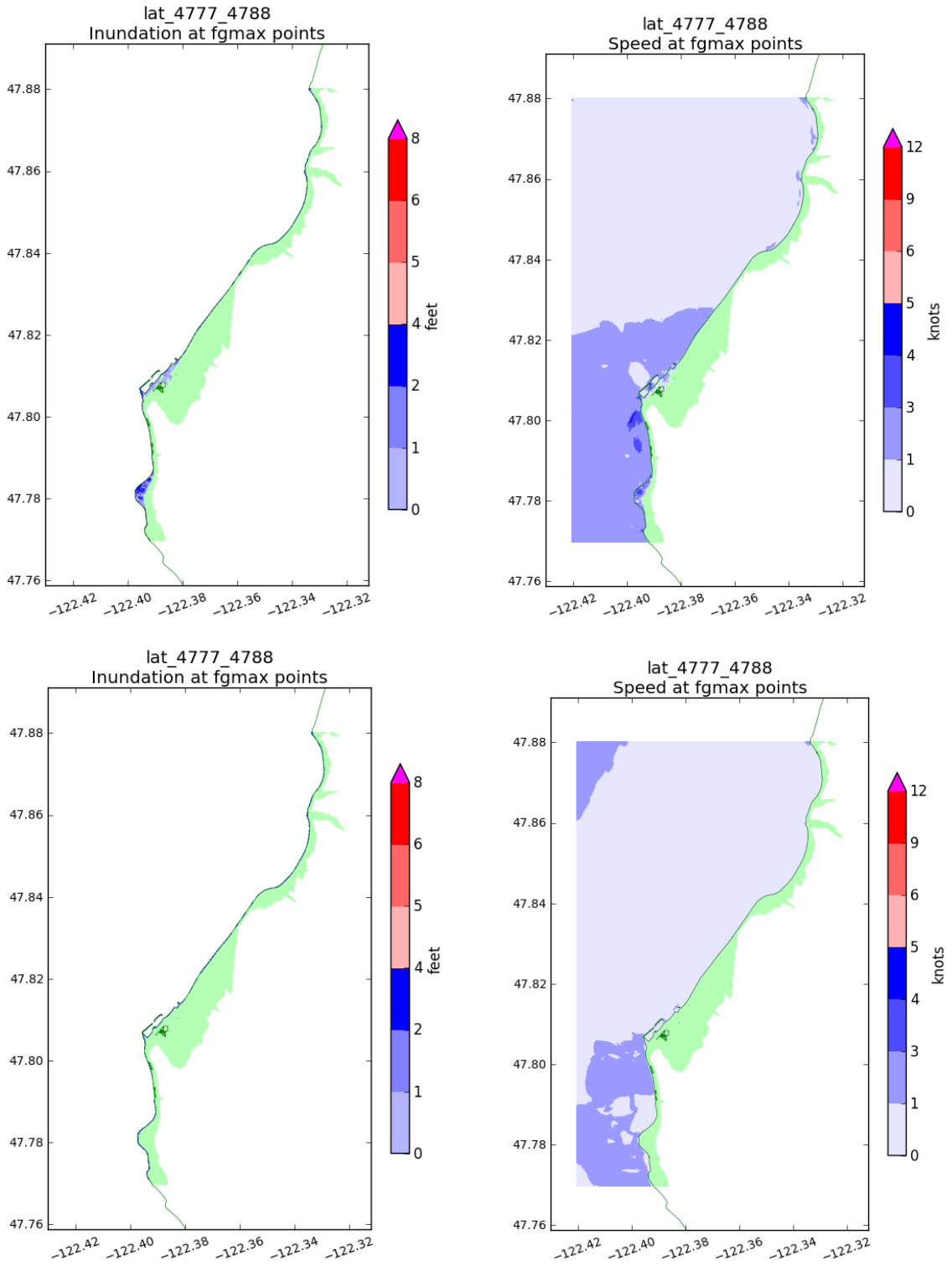

Figure 18: Sample results for the Region `lat_4777_4788`. Top: SF-L, Bottom: CSZ-L1, Left: Depth, Right: Speed.

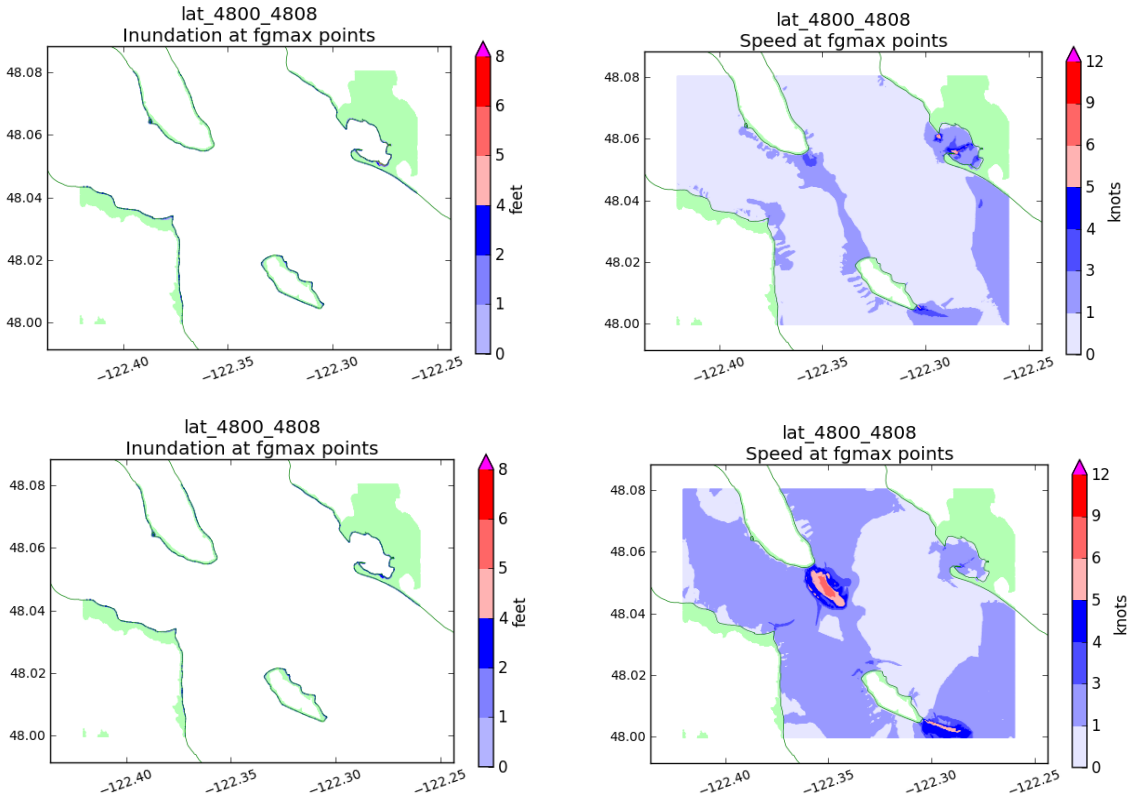

Figure 19: Sample results for the Region `lat_4800_4808`. Top: SF-L, Bottom: CSZ-L1, Left: Depth, Right: Speed.

7.3 Gauge output

Table 2 shows the location of simulated gauges used to capture time series of the flow depth / surface elevation and of the current velocity over the course of each simulation. The locations of the gauges are also indicated in Figures 6–10.

Gauges 6–11 were specified by DNR and the remaining gauge locations were chosen at points where the maximum current velocity was particularly large. Examining these gauges gives an indication that the run times chosen for these simulations were sufficiently long to capture the maximum depth and speed at each point.

Number	Longitude	Latitude	Location
6	-122.3980141	48.2512359	Skagit Bay south
7	-122.3861848	48.2248873	Port Susan
8	-122.2233282	47.9835954	Port Gardner east waterway
9	-122.3969815	47.9213880	Cultus Bay
10	-122.3069525	47.9479784	Mukilteo Lighthouse Park
11	-122.3858967	47.8134986	Edmonds Ferry Terminal
501	-122.4000000	47.8000000	South of Edmonds
502	-122.3820000	47.9010000	SE of Cultus Bay
503	-122.2260000	48.0300000	Priest Point
504	-122.2310000	48.0110000	Jetty Island
505	-122.3000000	48.0050000	SE of Hat Island
506	-122.3550000	48.0540000	SE of Camano Island
507	-122.2880000	48.0560000	Tulalip Bay
508	-122.4643000	48.1960000	Driftwood Shores Camano
509	-122.3705000	48.1940000	Stillaguamish River outlet
510	-122.4390000	48.2110000	Iverson Trail Camano
511	-122.3864000	47.9244000	Inner Cultus Bay

Table 2: Location of synthetic gauges.

The figures on the next few pages show gauge output from the gauges specified in Table 2. The time series for the gauges is available as csv files in the data products.

For each gauge, the figures below show the SF-L event on the top and the CSZ L1 event on the bottom.

The left panel in each figure shows the water elevation as a function of time, along with the GeoClaw topography value in the grid cell containing the gauge. This is generally constant in time and shows the initial depth of water at the gauge location. In the case of Gauge 10, which was onshore at an initially dry location, the interpolation algorithm changes once water arrives and so the apparent topography at this point changes slightly. However, the variation in surface elevation due to the depth of inundation is much larger than this small variation.

The right panel in each figure shows the current speed as a function of time along with the time history in the u–v plane, which shows how the direction of flow varies with time.

Note that the gauge plots for the SF-L event generally start at $t = 20$ seconds after the earthquake (which was assumed to have instantaneous displacement) and so the topography elevation shown by the green curves is the elevation after subsidence, if any. For the CSZ L1 event, the gauge time series generally start at 1.2 hours post-quake. There is no subsidence in Snohomish County from this event and so the GeoClaw topography elevation shown for this event is slightly larger than for the SF-L event for the southern gauges where the SF-L source gave subsidence.

Gauge 6: Skagit Bay south.

Computed on region `lat_4824_4831`.

SF-L event:

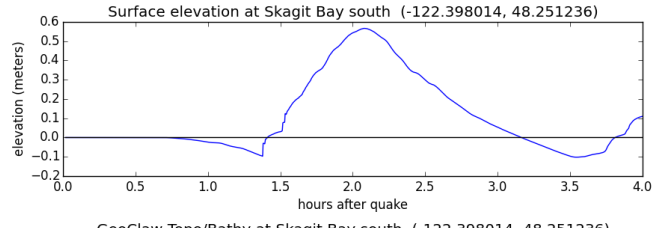

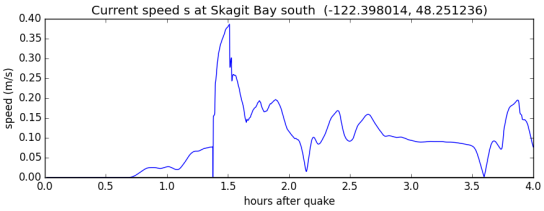

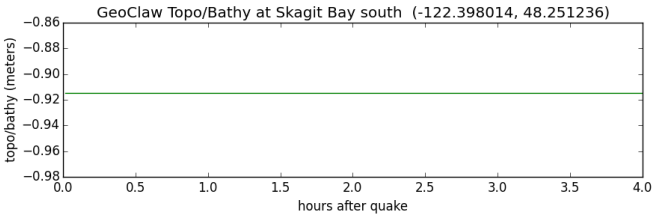

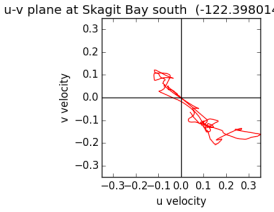

CSZ L1 event:

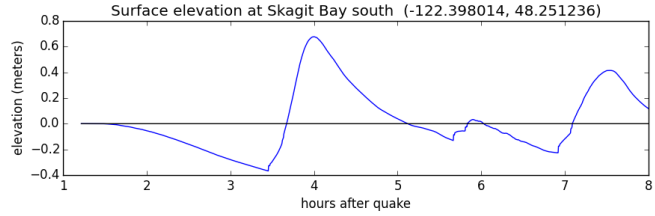

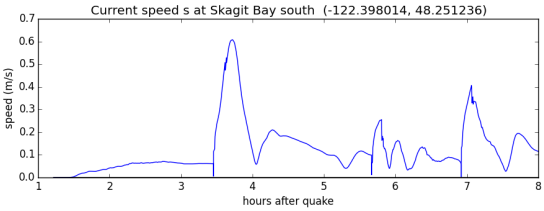

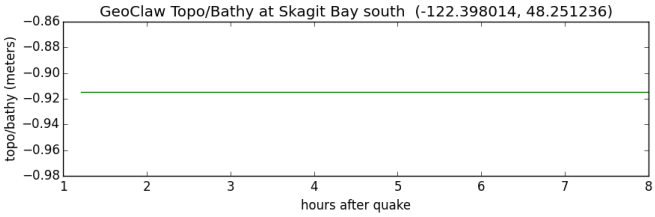

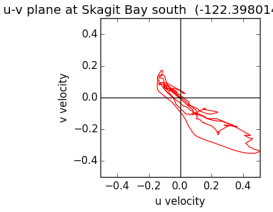

Gauge 7: Port Susan.

Computed on region `lat_4820_4825`.

SF-L event:

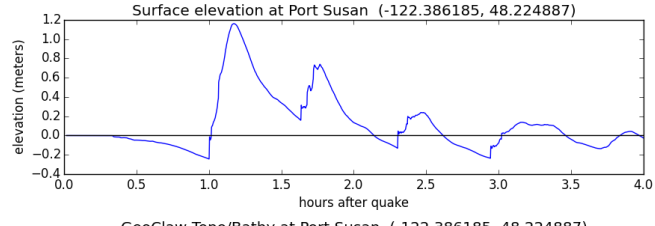

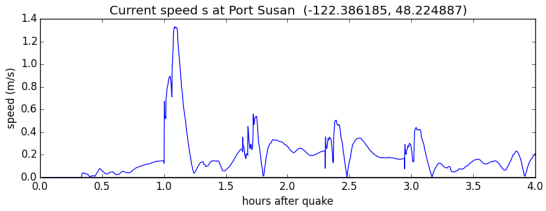

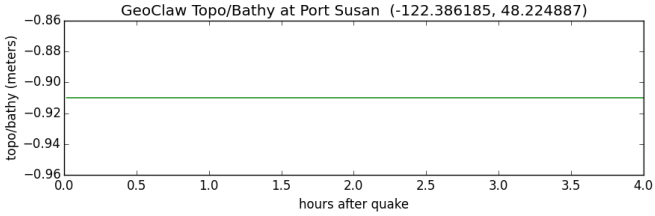

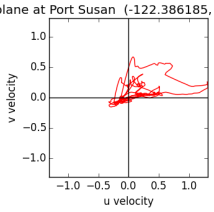

CSZ L1 event:

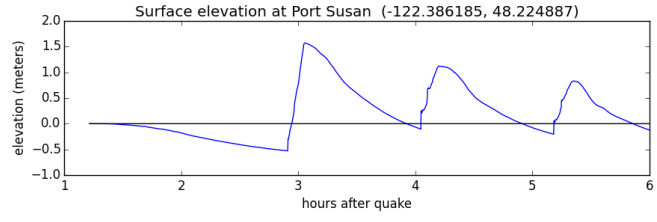

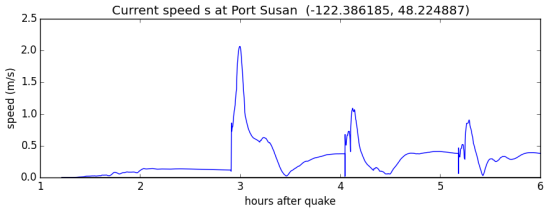

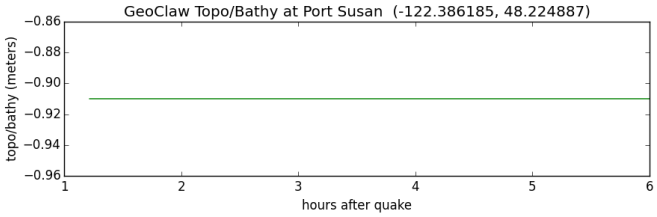

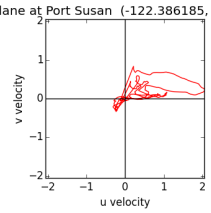

Gauge 8: Port Gardner east waterway.

Computed on region `lat_4795_4807`.

SF-L event:

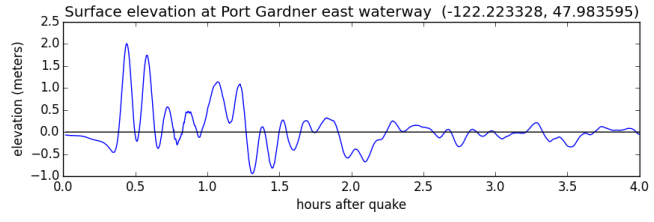

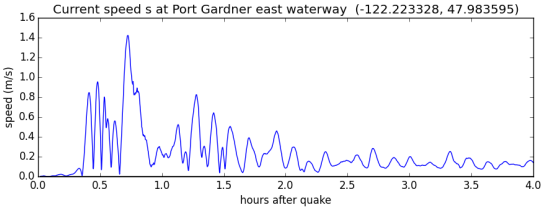

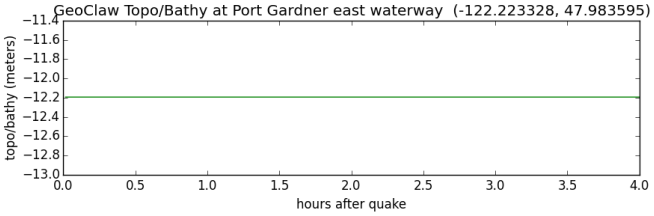

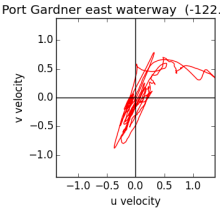

CSZ L1 event:

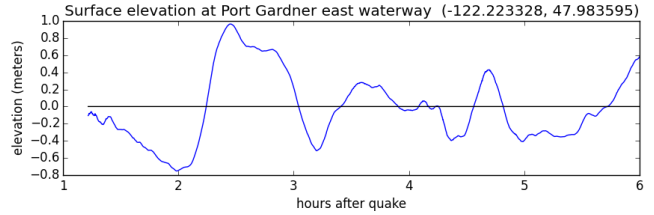

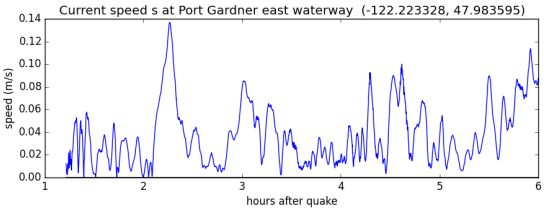

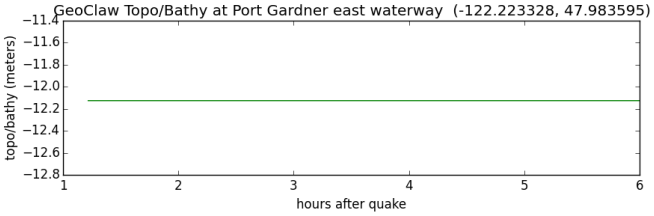

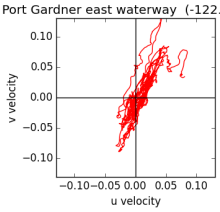

Gauge 9: Cultus Bay.

Computed on region `lat_4788_4795`.

SF-L event:

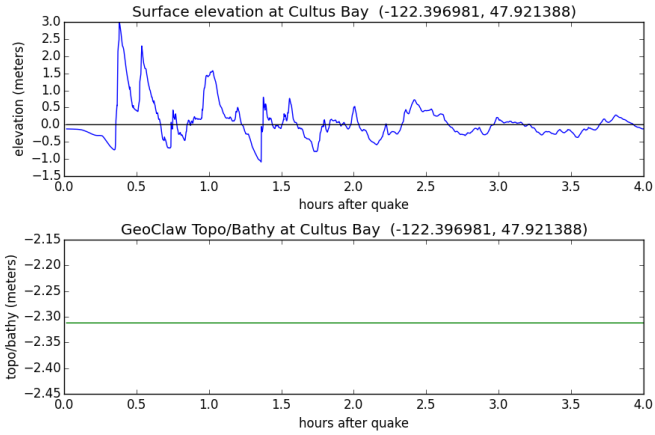

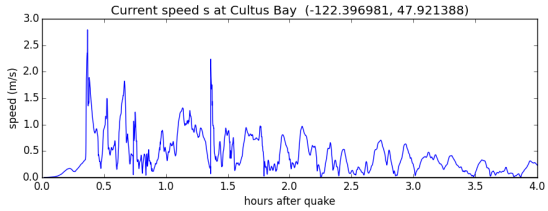

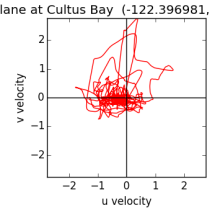

CSZ L1 event:

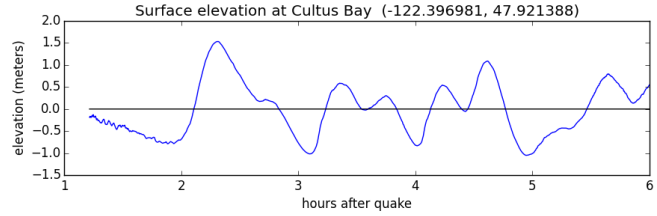

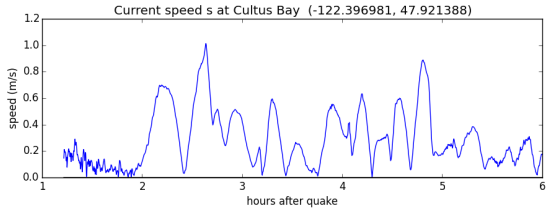

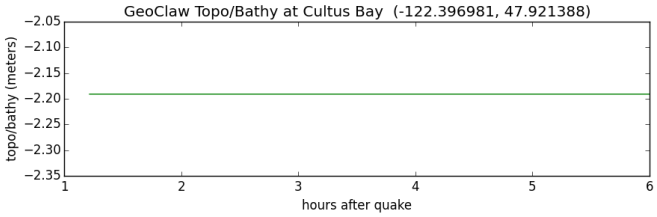

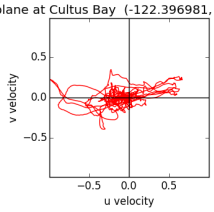

Gauge 10: Mukilteo Lighthouse Park.

Computed on region `lat_4788_4795`.

SF-L event:

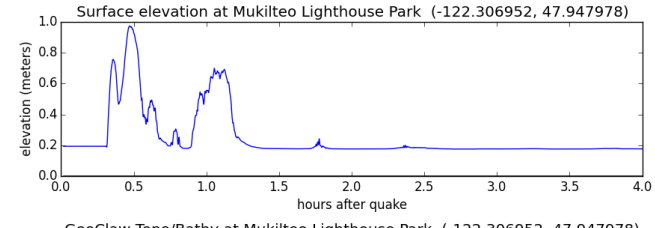

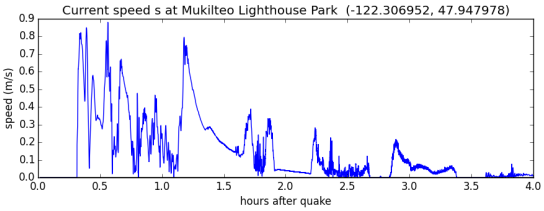

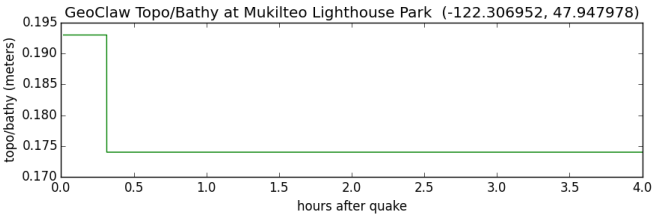

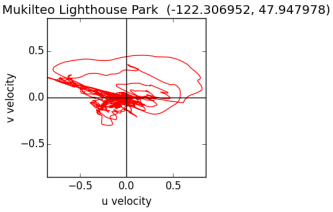

CSZ L1 event:

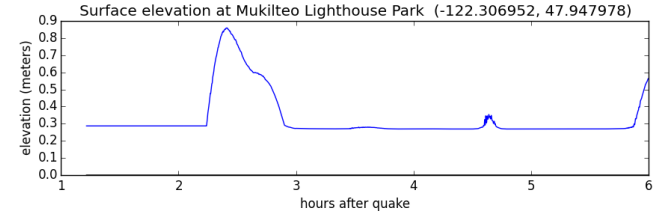

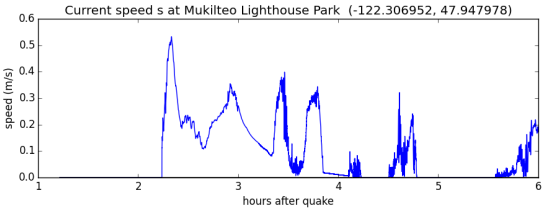

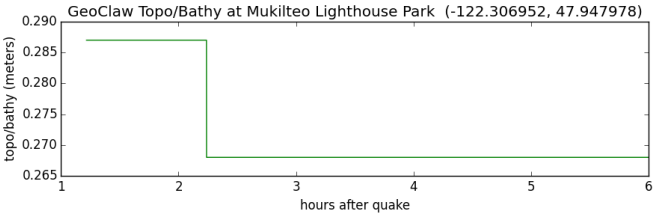

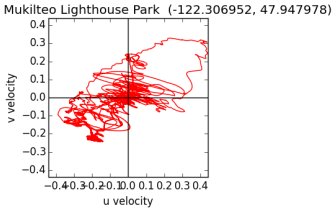

Gauge 11: Edmonds Ferry Terminal.

Computed on region `lat_4777_4788`.

SF-L event:

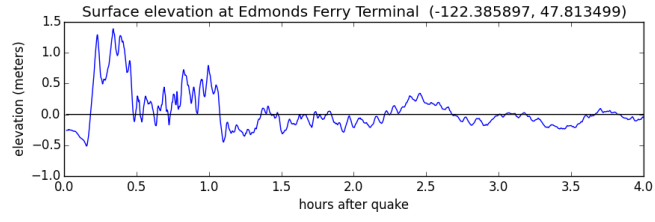

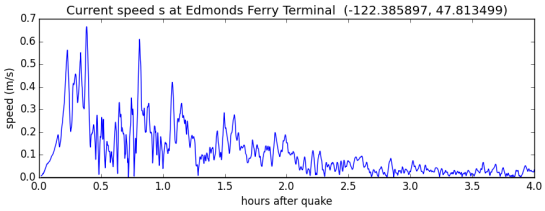

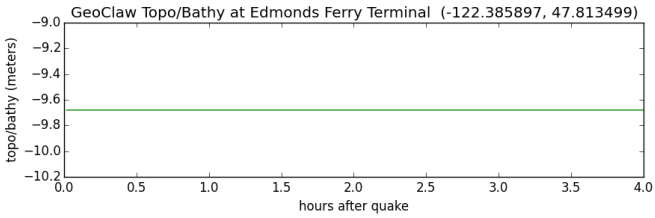

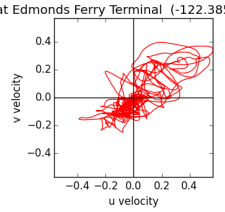

CSZ L1 event:

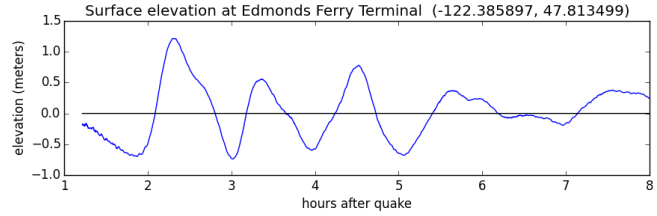

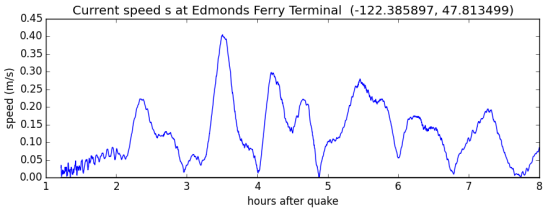

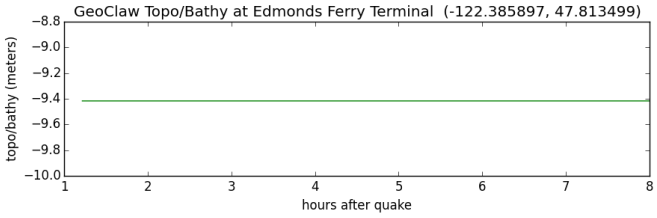

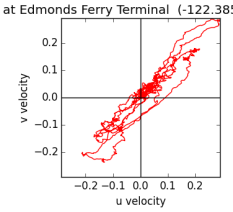

Gauge 501: South of Edmonds.

Computed on region `lat_4777_4788`.

SF-L event:

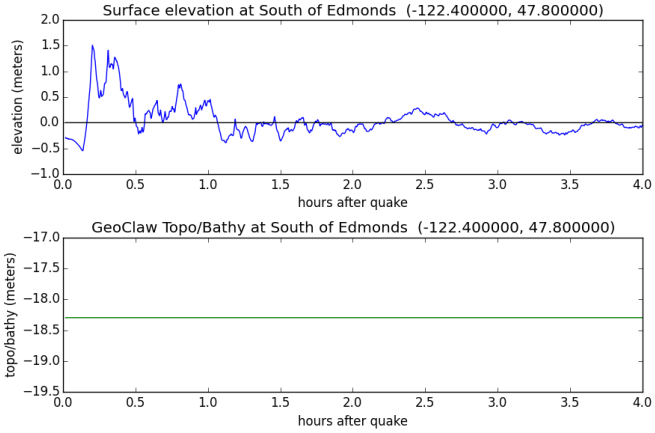

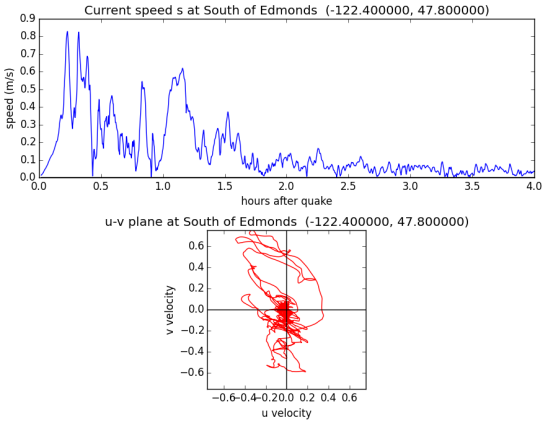

CSZ L1 event:

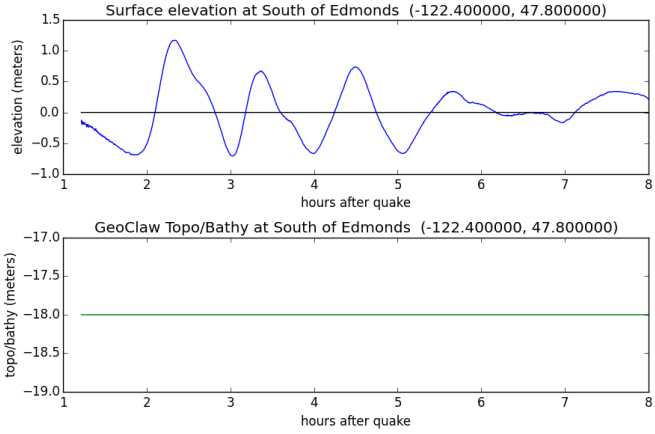

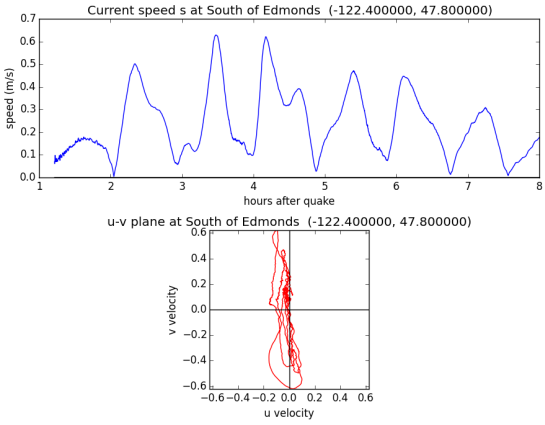

Gauge 502: SE of Cultus Bay.

Computed on region `lat_4788_4795`.

SF-L event:

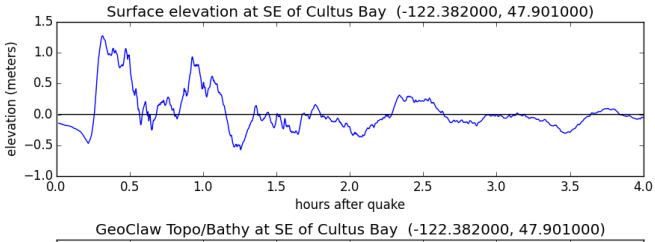

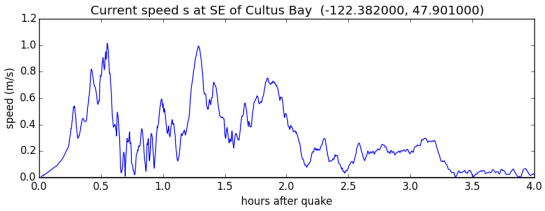

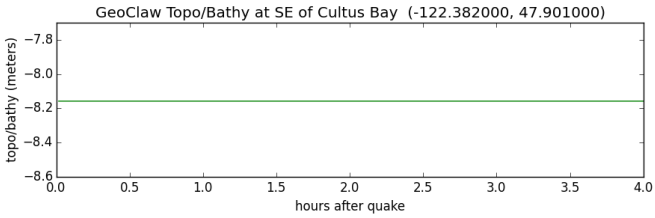

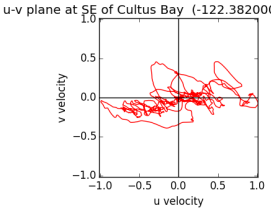

CSZ L1 event:

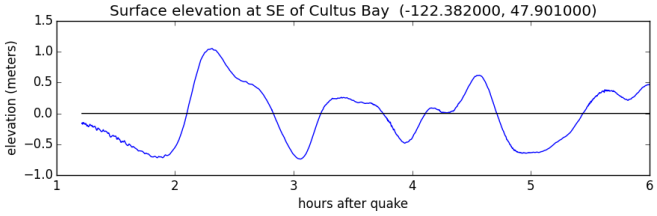

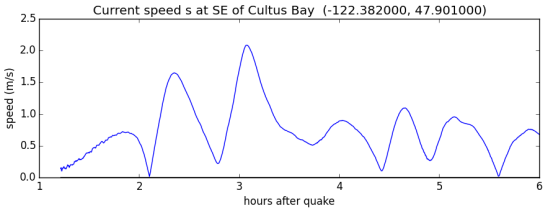

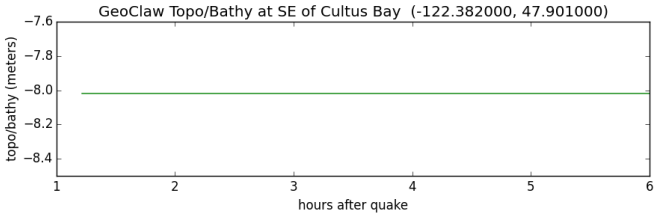

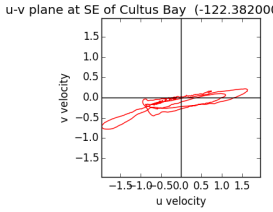

Gauge 503: Priest Point.

Computed on region `lat_4795_4807`.

SF-L event:

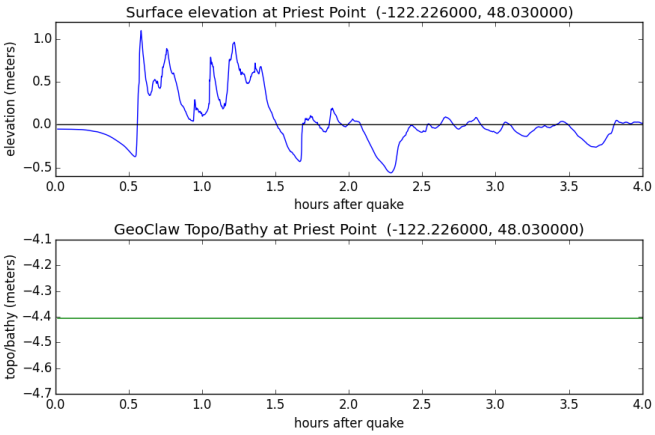

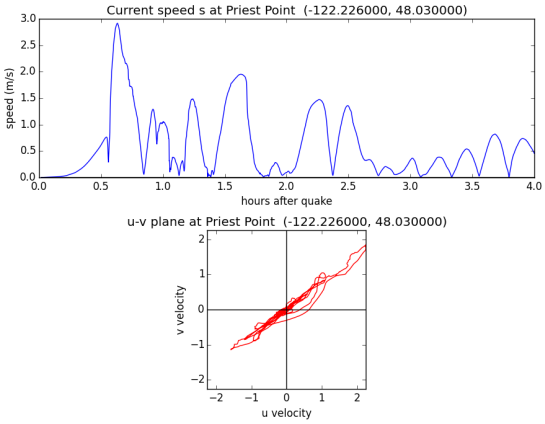

CSZ L1 event:

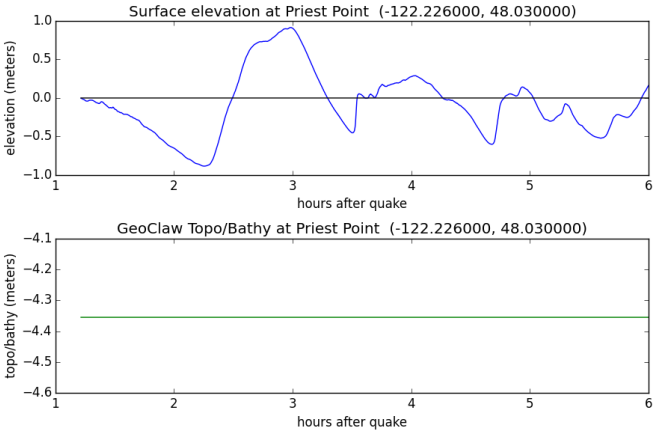

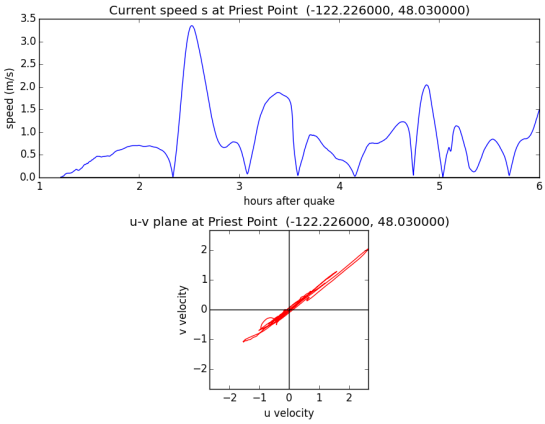

Gauge 504: Jetty Island.

Computed on region `lat_4795_4807`.

SF-L event:

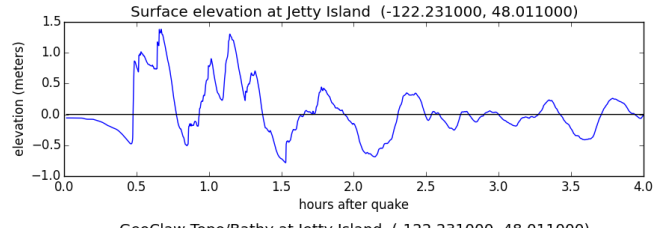

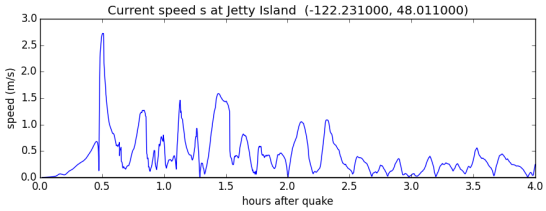

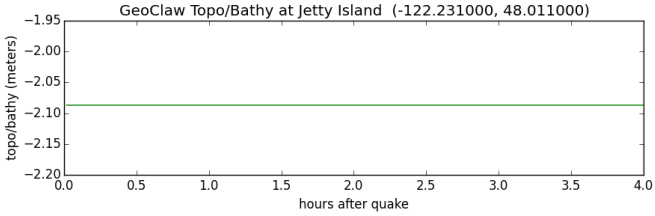

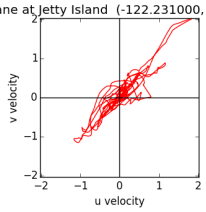

CSZ L1 event:

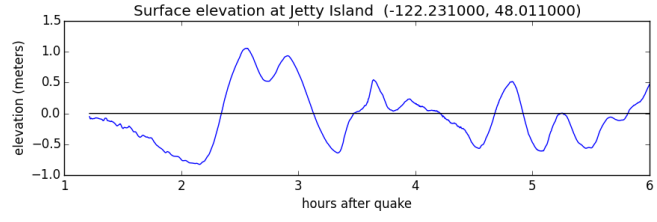

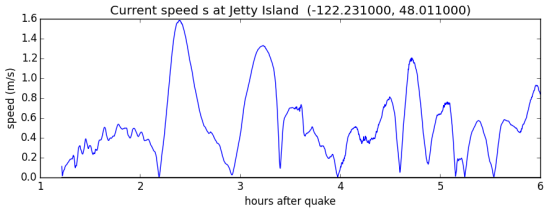

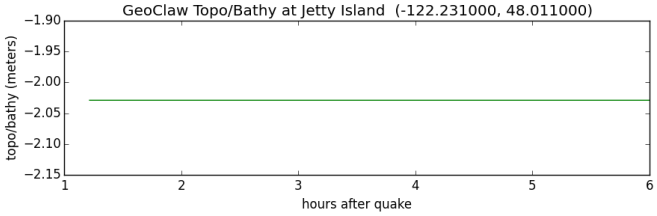

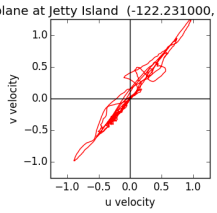

Gauge 505: SE of Hat Island.

Computed on region `lat_4795_4804`.

SF-L event:

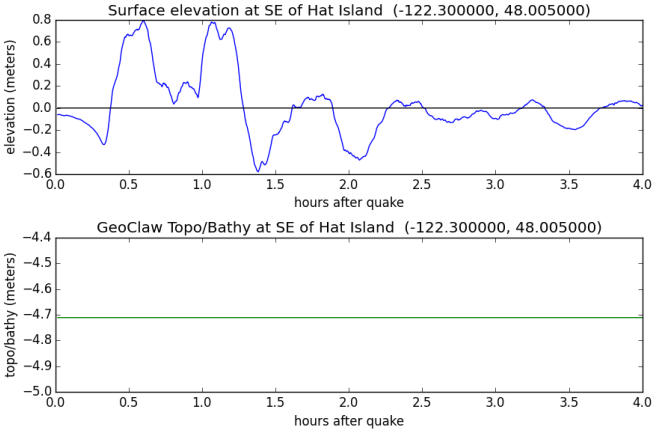

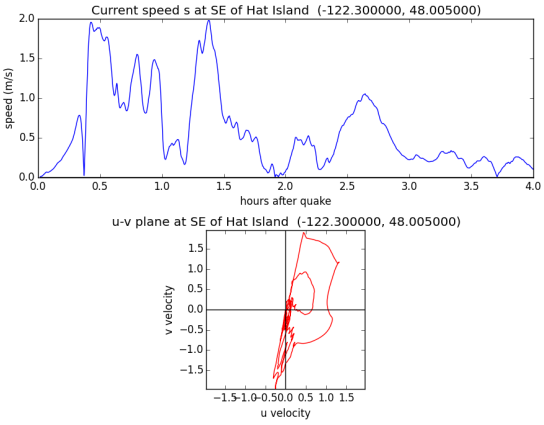

CSZ L1 event:

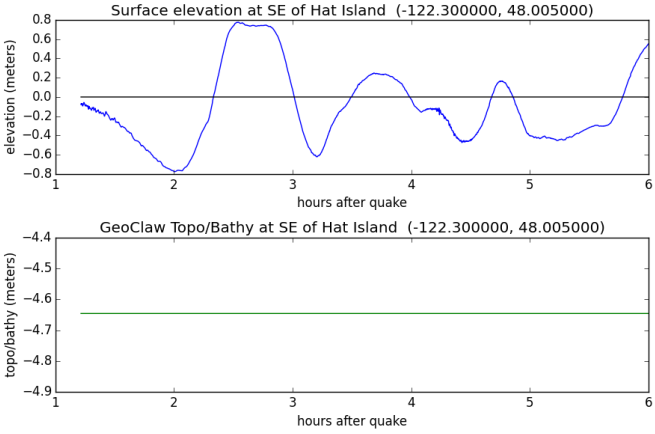

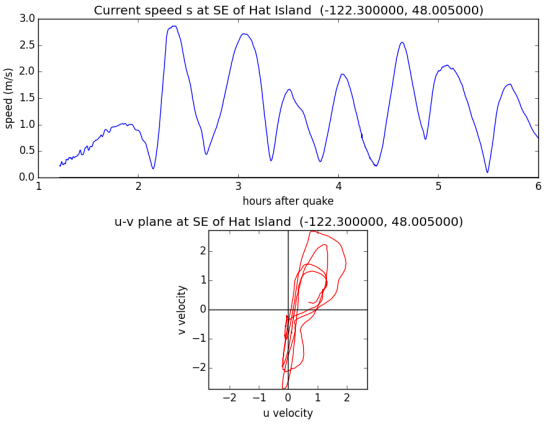

Gauge 506: SE of Camano Island.

Computed on region `lat_4800_4808`.

SF-L event:

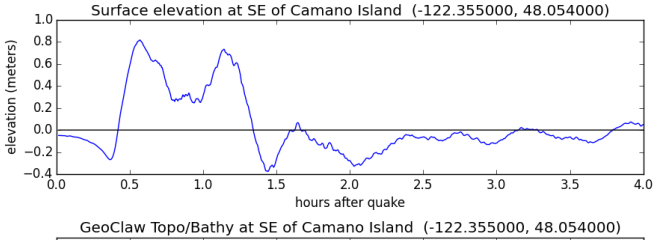

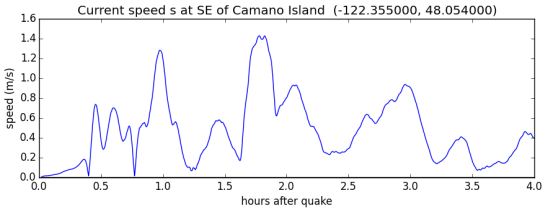

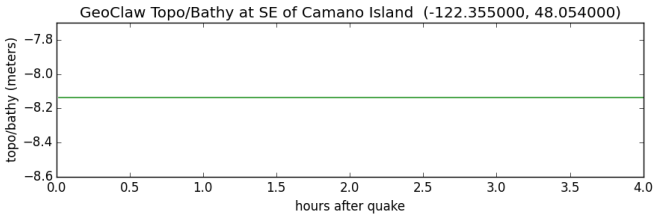

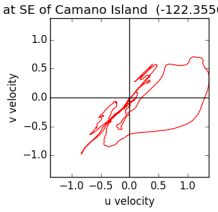

CSZ L1 event:

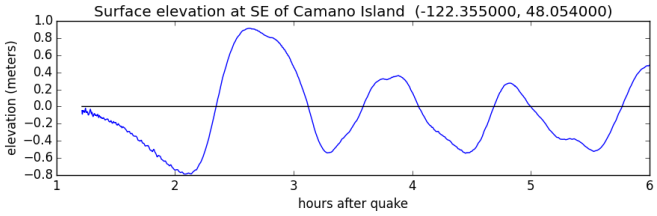

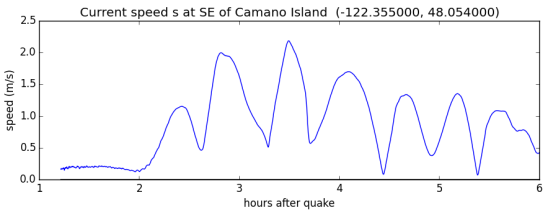

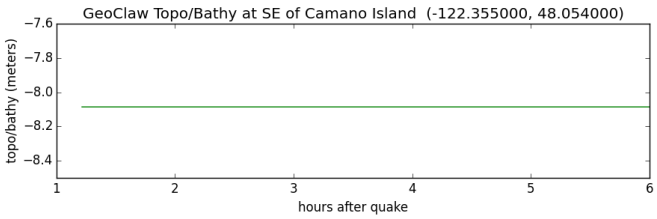

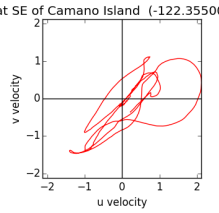

Gauge 507: Tulalip Bay.

Computed on region `lat_4800_4808`.

SF-L event:

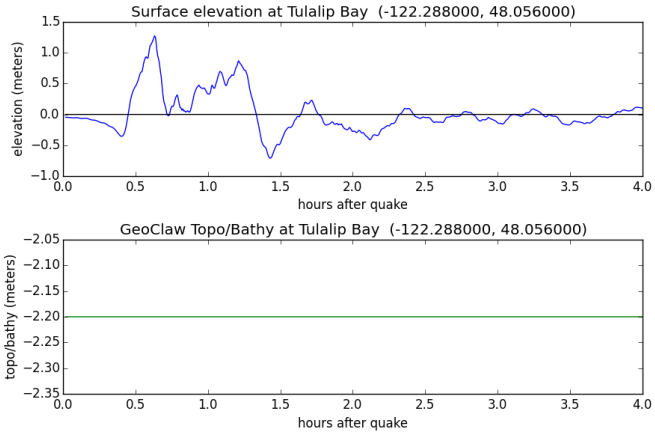

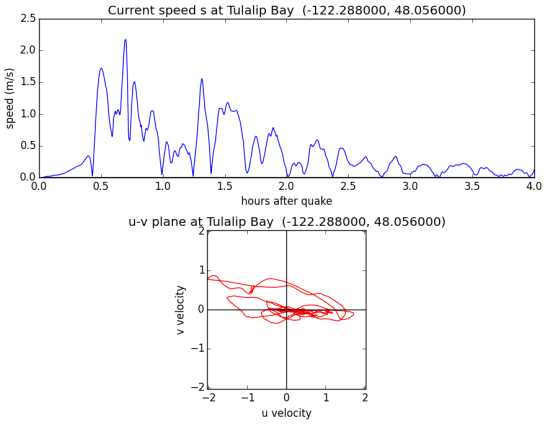

CSZ L1 event:

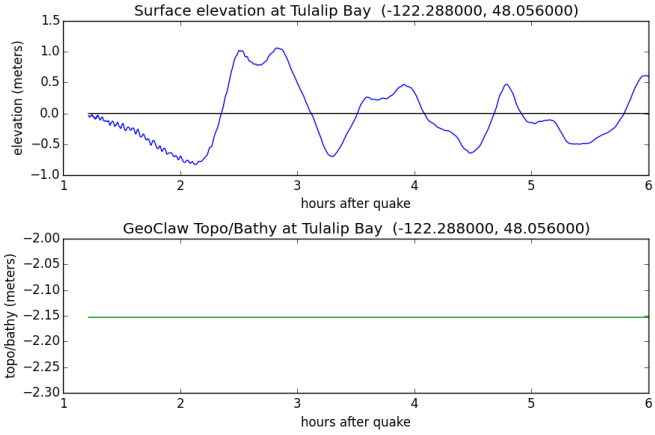

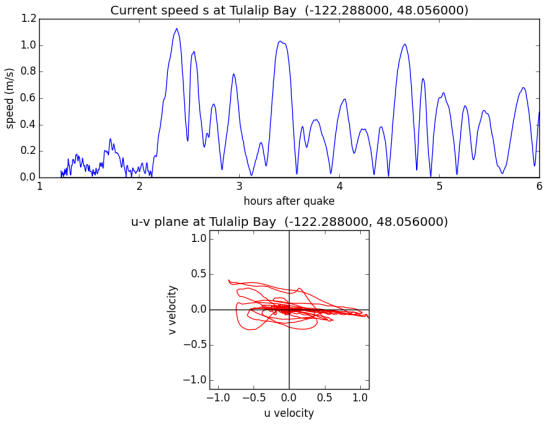

Gauge 508: Driftwood Shores Camano.

Computed on region `lat_4814_4820`.

SF-L event:

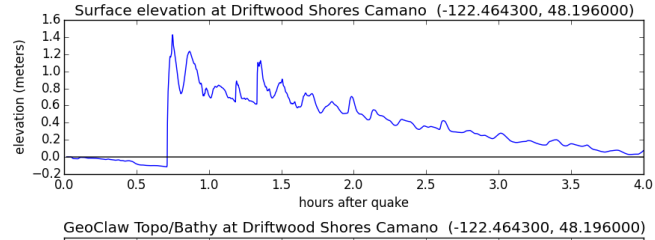

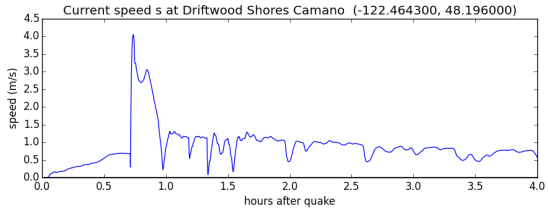

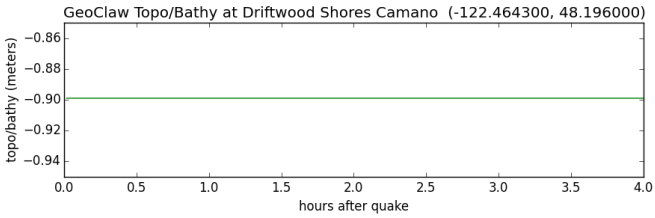

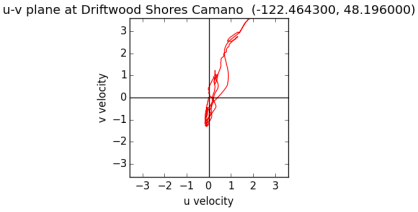

CSZ L1 event:

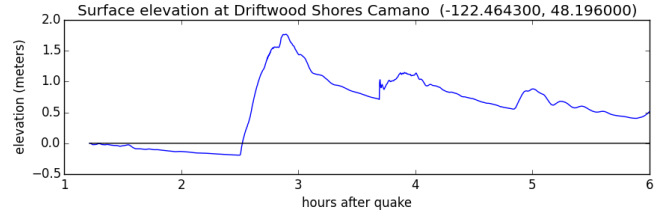

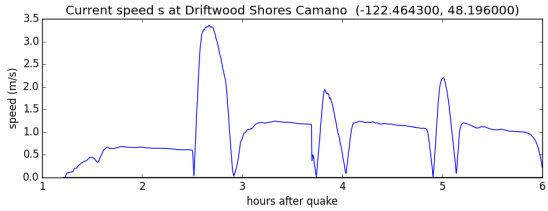

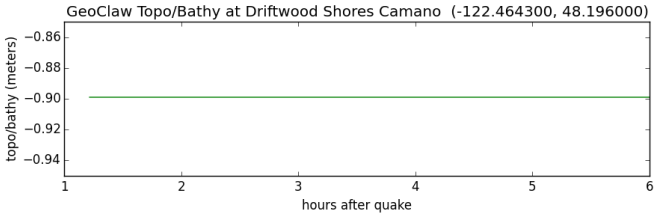

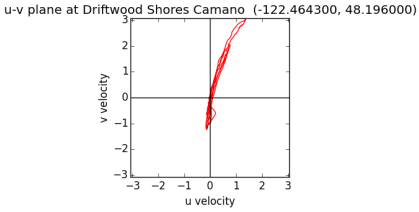

Gauge 509: Stillaguamish River outlet.

Computed on region `lat_4814_4820`.

SF-L event:

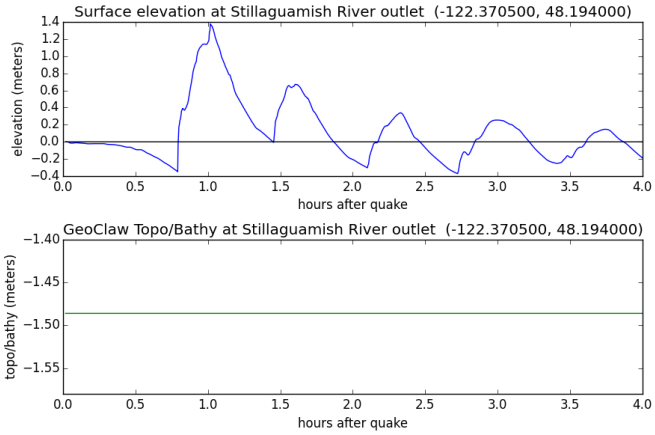

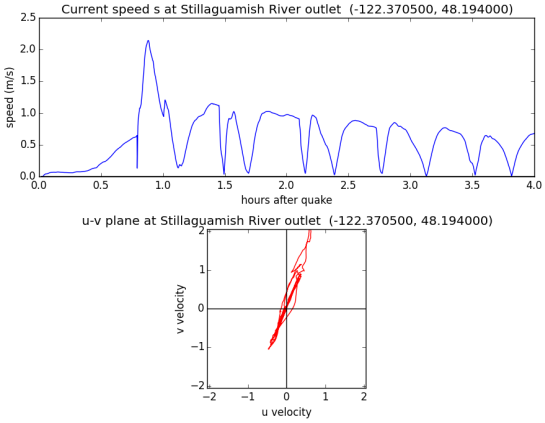

CSZ L1 event:

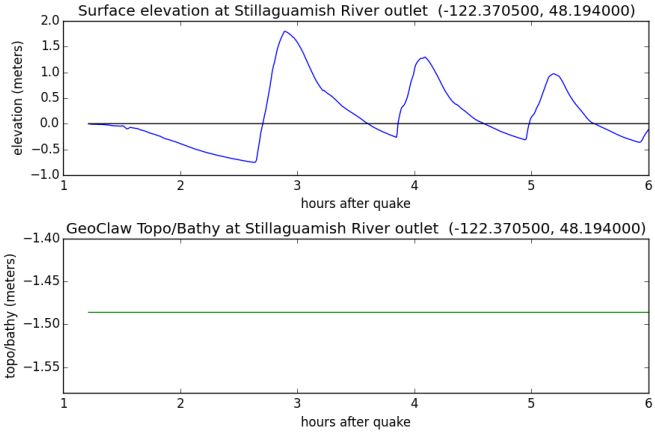

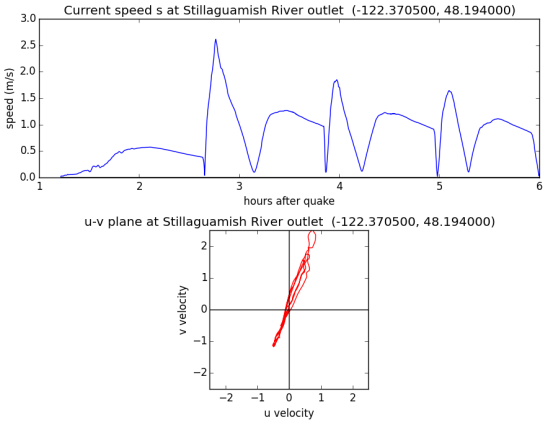

Gauge 510: Iverson Trail Camano.

Computed on region `lat_4820_4825`.

SF-L event:

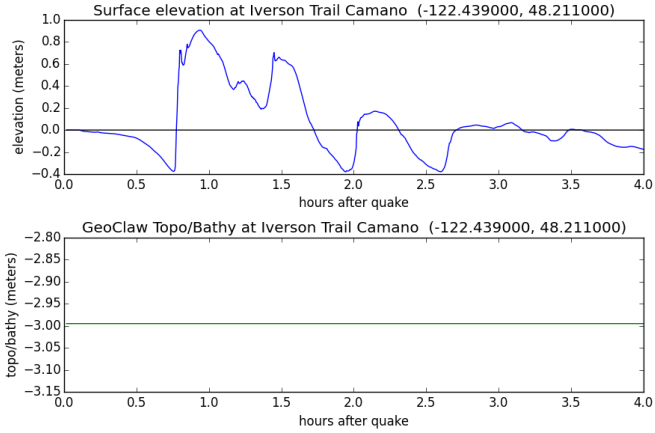

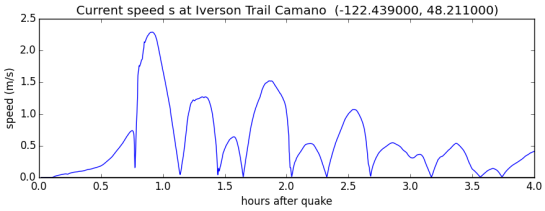

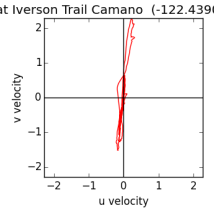

CSZ L1 event:

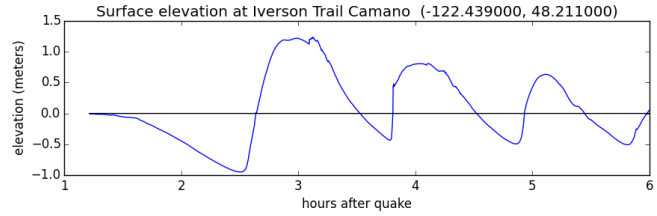

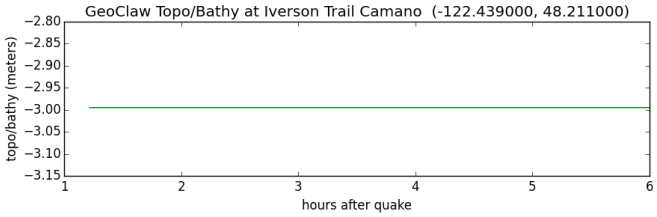

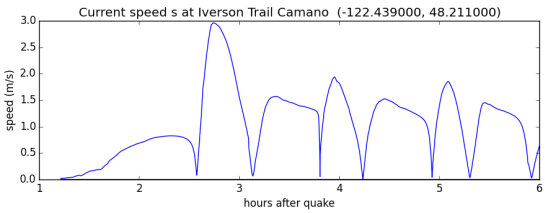

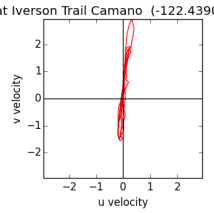

Gauge 511: Inner Cultus Bay.

Computed on region `lat_4788_4795`.

SF-L event:

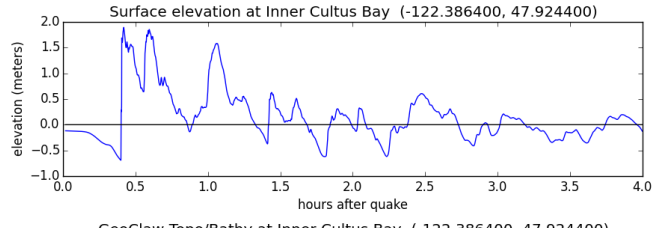

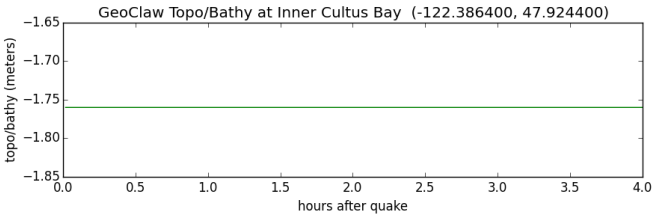

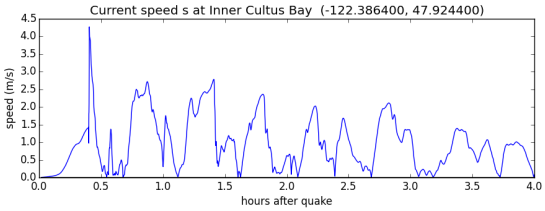

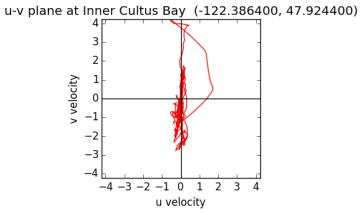

CSZ L1 event:

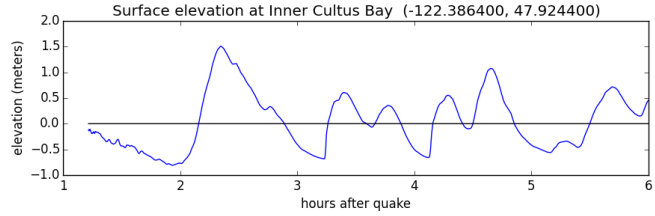

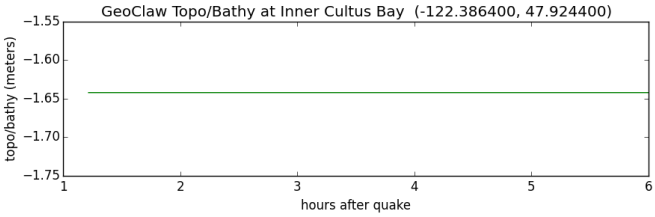

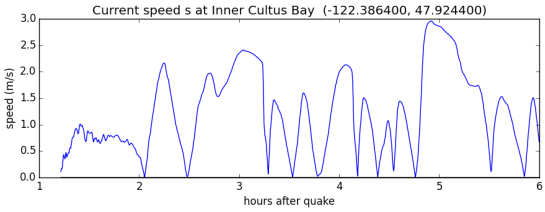

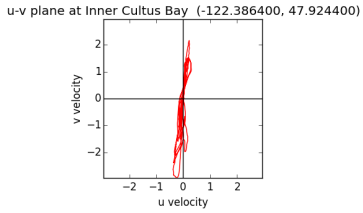

Appendices

A Modeling Details and GeoClaw Modifications

GeoClaw Version 5.5.0 was used for the modeling. This open source software is distributed as part of Clawpack, and is available from [4].

A few modifications were made to the software to deal with issues that arose in this modeling project. These are briefly described in this appendix and archived in the project Git repository. Some of these modifications will be incorporated into future versions of GeoClaw for more general use.

A.1 Generating fgmax points

Rather than defining a quadrilateral grid of fgmax points as has been done for past projects, in this project we selected points from the 1/3" DEM by filtering for all points in a specified rectangle (those shown in Figure 1) that (a) lie on the 1/3" by 1/3" subsampling grid and (b) have a topography elevation value z less than 40 m. This list of points, along with the z values, was saved to a file and used as the fgmax points. These z values were incorporated into the csv output files when postprocessing the model runs.

A.2 Grid registration

The DEMs used for this work are in ASCII raster format with cell-registration, as shown in Figure B of [19] (see also [5, 29]). The header for the data files includes `xllcorner, yllcorner`, the coordinates of the lower left corner of the grid. If the data are to be interpreted as values at points on a grid (rather than as cell averages), the `(i,j)` point (with 1-based indexing) should be interpreted as a pointwise value at `(xllcorner + (i-1/2)*cellsize, yllcorner + (j-1/2)*cellsize`, where `cellsize` is the width of the cell. The way this data is used in GeoClaw 5.5.0 to create topography in the finite volume cells, the data was incorrectly assumed to be pointwise values at points `(xllcorner + (i-1)*cellsize, yllcorner + (j-1)*cellsize`. A modified version of the GeoClaw `topo_module` was used to correct this, to obtain better correspondence with the maps that will eventually be produced. For the 1/3" DEMs, this results of a shift of only 1/6", or less than 5 m, but for the regions where there are very narrow dikes this may be important.

2" DEMs were created over the Puget Sound and Strait of Juan de Fuca regions by subsampling the 1/3" DEMs. The `xllcorner, yllcorner` values were properly adjusted in these files so that the points are properly registered relative to cell centers of this coarser grid.

A.3 Subsidence

Typically, subduction zone earthquakes are characterized by offshore uplift that generates the crest of an initial tsunami wave, nearshore subsidence that generates an initial tsunami wave trough offshore, and coastal subsidence that increases the depth and inland extent of subsequent flooding on land. The initial wave splits in two; one wave propagates into the open ocean, the other propagates toward a coastal region that has usually subsided and is therefore more susceptible to flooding. A crustal earthquake on the Seattle Fault creates uplift south of the fault and subsidence north of the fault.

For Snohomish County, there is no subsidence due to the CSZ L1 event, but parts of the County would experience subsidence from a Seattle Fault event. This is taken into account in the tsunami modeling. The topography deformation is used to modify the initial topography specified by the DEMs. This deformation changes the water surface and creates the tsunami, and also changes the topography in coastal regions. The water in Puget Sound is assumed to move with the topography over the short time scale of the earthquake, so initially the shoreline remains at the same location as both the land and the offshore water move vertically. But the new elevation of land near the shore can affect the extent of inundation, and regions that are now below MHW will eventually remain flooded (unless protected by dikes or levees).

There is a technical difficulty when using the GeoClaw adaptive mesh refinement (AMR) software in coastal regions that experience subsidence. Often the finest level grids (the 1/3" by 1/3" computational

grids in this project) are not introduced in a region until shortly before the tsunami arrives (in order to reduce computatonal time). When the coastal region is eventually refined, the grid cells must be initialized with a depth of water that is appropriated for undisturbed water at this location. The routines built into GeoClaw 5.5.0 will fill these cells by choosing the depth h so that $B + h = 0$, where B is the cell-averaged topography value and 0 corresponds to MHW for the 1/3" DEMs provided by NCEI. However, if there has been subsidence Δz in this region, then the water was assumed to move with the topography by this vertical displacement, and so h should instead be chosen so that $B + h = \Delta z$. This improvement was made to the GeoClaw code for this project and will be incorporated into future versions of GeoClaw.

B Mismatch of 1/3" DEMs

Figure 20 illustrates the mismatch of 1/3" Puget Sound [17] and Port Townsend [16] DEMs. The merged DEM provided by NCEI for this project agrees with the Puget Sound DEM in the Everett region, and transitions to agree with the Port Townsend DEM to the north, matching up at latitude 48.2N as illustrated in Figure 5.

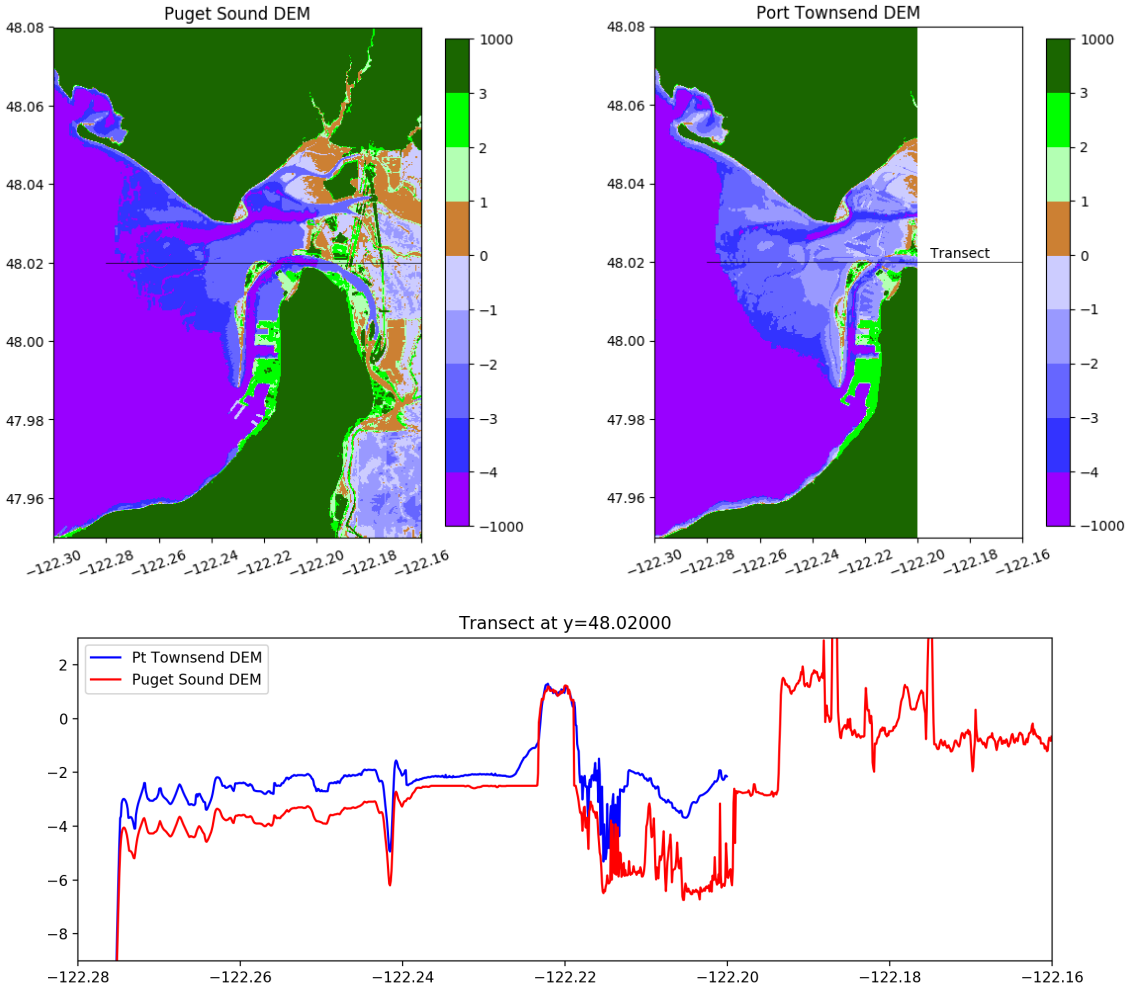

Figure 20: Comparison of the Puget Sound (PS) 1/3" DEM and Port Townsend (PT) 1/3" DEM near Everett. Note that the PT DEM ends at longitude −122.20.

C Towards more proper modeling of dikes

Figure 21 shows part of Port Susan south of Stanwood. In the lower plots, all the brown regions are below MHW. Some of these regions are behind dikes and should be initially dry, and should stay dry if the tsunami does not overtop the dike. With the standard GeoClaw initialization as used in this project, all brown regions are initially filled with water to MHW, as discussed in Section 4 and seen in Figures 6 and 7. By initializing a simulation with water level $h + B = -3$ meters and then slowly raising the sea level, it is possible to fill only the regions that are directly connected to the bay with water, as shown in the lower right plot. This simulation was done on a 1/3" by 1/3" grid and still there is one region marked in the plot where the dike is not well enough resolved to keep water out of a region that should be dry. When the 2/3" by 1/3" grids desired for this project are used, additional gaps in the dikes appear and additional areas that should be dry fill with water. This initialization procedure is still under development and is not yet coupled into the full GeoClaw adaptive grid solution procedure. (Note: This section unchanged from Version 1 of report.)

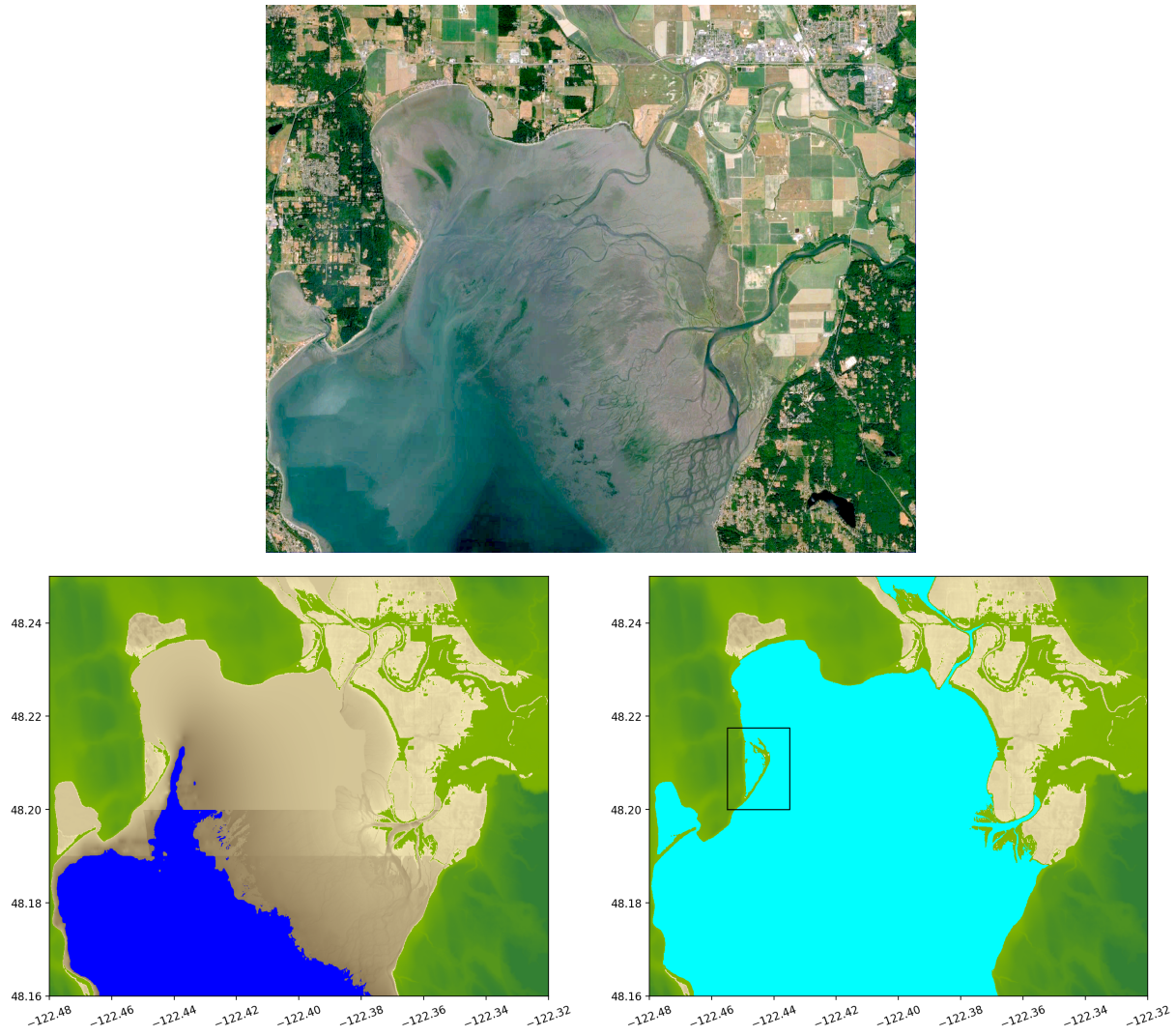

Figure 21: Top: Google Earth image of Port Susan south of Stanwood. Bottom left: Topography with fluid filled only to −3 m below MHW. Bottom right: After letting water raise slowly to MHW. The brown areas are below MHW. The boxed area shows a point just south of Livingston Bay that should be dry but where water leaks in due to a gap in the dike in the computational grid topography.

D CSZ L1 model comparisons

The comparisons shown in this section are taken from the original work done on 2/3" by 1/3" grids, and has not been redone on 1/3" by 1/3" resolution.

Figure 3 shows two different versions of the CSZ L1 deformation. To check that the choice of deformation makes little difference in the results, we ran some simulations with both versions. Figure 22 shows a comparison or results in region `lat_4795_4807`, near Everett.

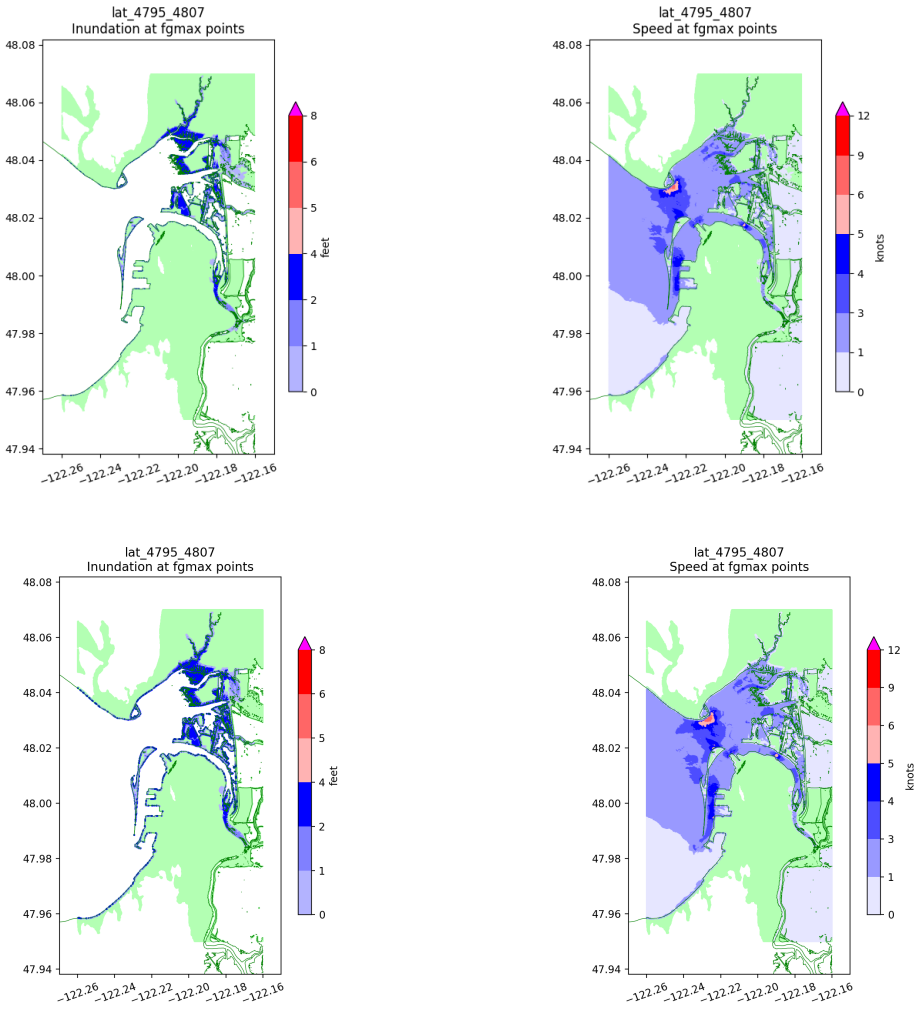

Figure 22: Results near Everett using the CSZ L1 event. The top row shows results with the version of L1 provided by PMEL, which was used to produce the published results for all regions. For comparison, the bottom row shows the results are very similar when the UW extension of L1 is used instead.

E Seattle Fault scenario issues

In five Seattle Fault tsunami modeling studies published during the period 2001–2015 [3, 12, 13, 25, 26], there appear to be inconsistencies in the fault plane models that were applied, perhaps due to evolving understanding of the fault structure. Koshimura et al. [12, 13] developed a fault model according to the structure inferred by [21] and [11]. In addition to these reports, guidance for development of the later models [3, 25, 26] was provided by (a) the 2002 report updating the National Seismic Hazard Maps [6], (b) a joint NOAA/USGS/WADNR/WAEMD 2002 Workshop to develop quantitative descriptions of potential tsunamigenic earthquake, landslide and delta failure events in Puget Sound [10], (c) a 2007 study of Seattle seismic hazards [7] and (d) discussions with the authors of these reports.

The 2002 Workshop focused on development of earthquake models for two Seattle Fault events described by Frankel et al. [6]; the first, an Mw $>$ 7 magnitude with recurrence period $\sim$ 5000 years, the second was a smaller Mw $>$ 6.5 with recurrence of $\sim$ 1000 years (see Table 2.1 of [10]), which we here refer to as SF-L and SF-S, respectively. In the reports cited above they are referred to as Mw 7.3 and Mw 6.7 events, but we have found in many cases that the reported values of the fault parameters produce events with different magnitudes.

E.1 The SF-L event

The SF-L event was designed to model the earthquake that occured roughly 1100 years ago, and for which geologic data is available for the uplift or subsidence at several locations, in particular Restoration point (7 m), Alki Point (4 m), and West Point (-1 m). The original tsunami source was designed by Koshimura et al. [12] based on seismic reflection data of Pratt et al. [21] and consisted of 12 subfaults, 6 shallow ($\leq$ 5.5 km) and 6 deep ($\geq$ 5.5 km) segments. The shallow segments dip at 60° and the deep ones at 25°. It is not clear why these dip angles were chosen, since in [21] it is stated that the fault dips at about 20°, steepening to 45° near the surface. The shallow subfaults have width 6 km and the deep ones have width 38 km. The depth of the subfaults below the surface is not given. Koshimura et al. [12] used this set of subfaults to generate surface displacement (via the Okada model) and report deformation that agreed well at the three locations mentioned above. They also performed tsunami simulations using the TUNAMI-N2 code, comparing results at Cultus Bay on Whidbey Island to observed tsunami deposits. Unfortunately, [12] does not contain all the subfault parameters needed to reproduce this deformation. In addition to the missing depth, the latitude and longitude of each subfault is not precisely specified.

Frankel et al. [6] describe an "Mmax" 7.3 earthquake on the northern trace of three faults in the Seattle Fault zone, assuming "... faults strike east-west, dip at 45 degrees, and with a 20 km seismogenic thickness ...". The model of [12] was simplified by PMEL in consultation with DNR to obtain a 6-subfault model that was used in a 2003 tsunami hazard analysis of Seattle in PMEL-124 [25] and appears in Table 1 of that report. The magnitude was scaled back from the Mw 7.6 event of [12] to what was claimed to be a Mw 7.3 event (although we find Mw 7.39). In this model the subfaults have width 20 km and dip 60°, rather than the 45° dip mentioned by Frankel et al. [6]. The depth below the surface is not specified. The 60° dip is justified as "within the uncertainly range of many recent fault models", citing ten Brink et al. [24] and other studies. Slip on these subfaults was chosen to match the observations at the three locations cited above, and compared in Table 2 of [25]. Unfortunately the latitude and longitude of each subfault is not specified in this or later PMEL reports, but we have determined the position of the top-center of each subfault from discussions with PMEL and examination of past results. Table 3 gives our estimates of these values, along with the other subfault parameters that were unchanged between studies.

Essentially the same subfault model was used in the 2007 study of Tacoma in PMEL-132 [26]. However, the width of each subfault was increased from 20 km to 35 km. This was presumably done in light of work done in the meantime that suggested the fault may extend lower than 20 km.

Although the fault width was increased, the slip on each subfault was kept the same as in Table 3. This changes the magnitude of the earthquake, which is based on the logarithm of the seismic moment, defined by

$$Mo = \mu \sum_j W_j L_j D_j \tag{1}$$

This sum is over all subfaults j, with length L_j, width W_j, and slip displacement D_j. The rigidity (shear modulus) μ was taken to be 30 GPa in Koshimaru [12] and is not stated in later studies. If the units of W_j, L_j, D_j is meters, then Mo is in Newton-meters (Nm) and the moment magnitude is then given by

$$\text{Mw} = \frac{2}{3}(\log_{10}(Mo) - 9.05). \tag{2}$$

Koshimaru [12] used a variant of this with 9.05 replaced by 9.1, which often appears in the literature and gives a value for Mw that is smaller by 0.033. The formula (2) is considered more correct[1] and agrees with the expression $\text{Mw} = \frac{2}{3}(\log_{10}(Mo) - 10.7$ for the case when Mo is measured in dyne-cm (1 dyne-cm = 10^7 Nm). Table 4 shows the magnitude that we compute using (2) for each of the past studies cited, in the lines labelled "our result".

By increasing the fault width by a factor of 35/20 while keeping the slip the same, the magnitude of the earthquake is changed by $\frac{2}{3}\log_{10}(35/20) \approx 0.162$.

On the other hand, since the new slip is added deep in the earth relative to the original slip, this increase actually causes relatively little difference in the surface deformation (and hence in the tsunami generated).

Table 4 also shows our computation of the deformation at the three points where observations are available, compared to the values that were reported in the past PMEL studies where these values were provided. We used the version of the Okada model developed as part of GeoClaw. We cannot explain yet why we get different values than the original studies.

A further mystery is why the fault deformation shown in Figure 2 of PMEL-124 [25] seems to match the contours we compute using a fault width of 35 km rather than the width 20 km recorded in [25].

A question for future studies: Should the fault width be set back to 20 km? If it is kept at 35 km, do we now say this is a Mw 7.5 event rather than Mw 7.3? If the width should be 35 km but the goal is still to model a Mw 7.3 event, then the slip should be scaled down on this wider fault by a factor of roughly 20/35. In fact we find scaling by a factor of 0.5 gives Mw 7.35, due to use of the formula (2). This event has significantly less surface deformation than the SF-L event used in past studies since less of the slip will be near the surface. The final row in Table 4 shows these values.

Subfault	Longitude	Latitude	Length	Strike	Slip
A1	-122.7599344	47.6115777	15.2 km	87.9°	1 m
A2	-122.6165584	47.6157655	6.3 km	86.6°	1 m
A3	-122.5154909	47.6132604	8.9 km	96°	12 m
A4	-122.4397627	47.6000508	3.3 km	128.8°	11 m
A5	-122.3474066	47.5826645	11.5 km	99.3°	4 m
A6	-122.1735094	47.5847905	14.9 km	81°	1 m

Table 3: Seattle Fault SF-L. This table shows the primary parameters that seem to be unchanged between different past studies. A dip of 60° has been used for all subfaults in past studies. The longitude and latitude is for the top center of the subfault, and has been inferred from the literature. The width used varies between studies.

[1] https://earthquake.usgs.gov/learn/topics/measure.php

Study	Model parameters		Deformation			
	Width	Magnitude	Alki Pt.	Restoration Pt.	West Pt.	Max
Observations [12]			4 m	7 m	-1 ± 0.5 m	
Koshimaru [12]	vary	7.6	4.2	5.3	-0.22	
Our result	vary	7.61				
PMEL-124 [25]	20	7.3	3.9	7.1	-1.3	
Our result	20	7.39	3.52	6.66	-0.97	8.05
PMEL-132 [26]	35	7.3	3.6	7.2	-1.1	
Our result	35	7.54	3.76	6.93	-1.10	8.16
Slip halved	35	7.35	1.88	3.46	-0.55	4.08

Table 4: Seattle Fault SF-L. This table shows the observed uplift or subsidence (deformation) at three locations, as reported in [12], followed by the results from three past modeling studies. The Koshimaru results were from a model with 12 subfaults. The PMEL-124 [25] and PMEL-132 [26] studies used the same parameters from Table 3, but the subfault width was increased from 20 to 35 km. The rows labelled "our result" show the magnitude we compute from (2) and, for the latter two studies, the deformation we compute from the Okada model implemented in GeoClaw using the same parameters as in each original study. We assumed all subfaults were at a depth of 500 m (top of fault to surface). The final row shows values we obtain if the slip from Table 3 is halved on each subfault to counterbalance the increase in width.

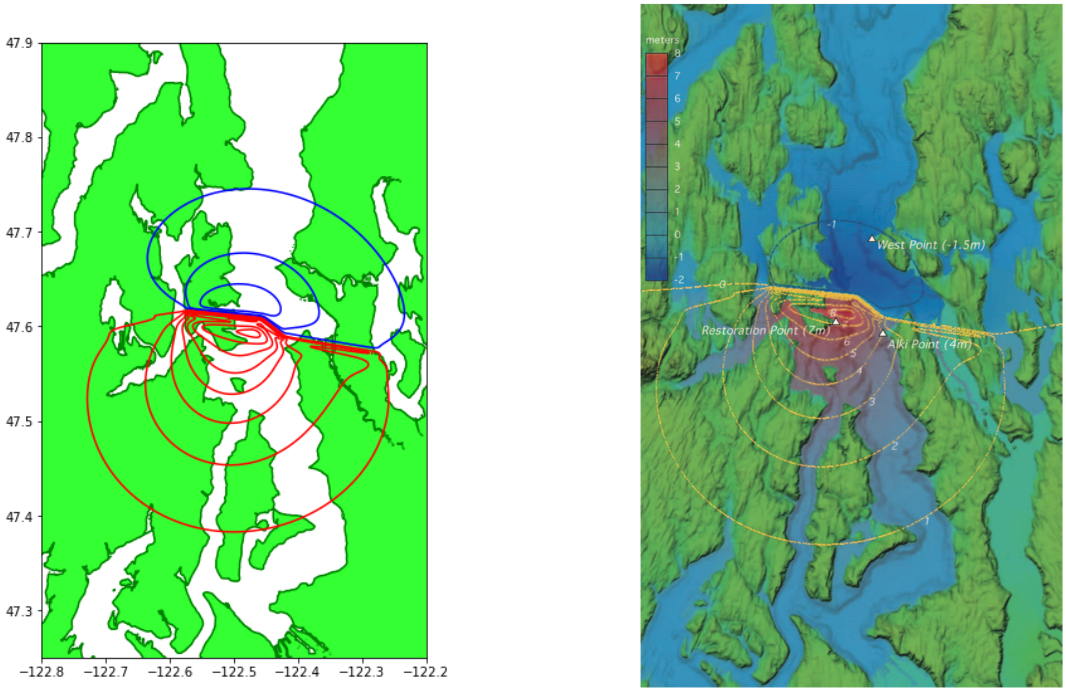

Figure 23: Left: SF-L deformation provided by PMEL and used in Snohomish County study. Right: Figure 2 from PMEL-124 [25]. Note that the contours in the figure on the right match well with those on the left and with those of Figure 24, and not so well with those shown on the left in Figure 25. This suggests a fault width of 35 km might have been used in [25], contrary to the table in that report.

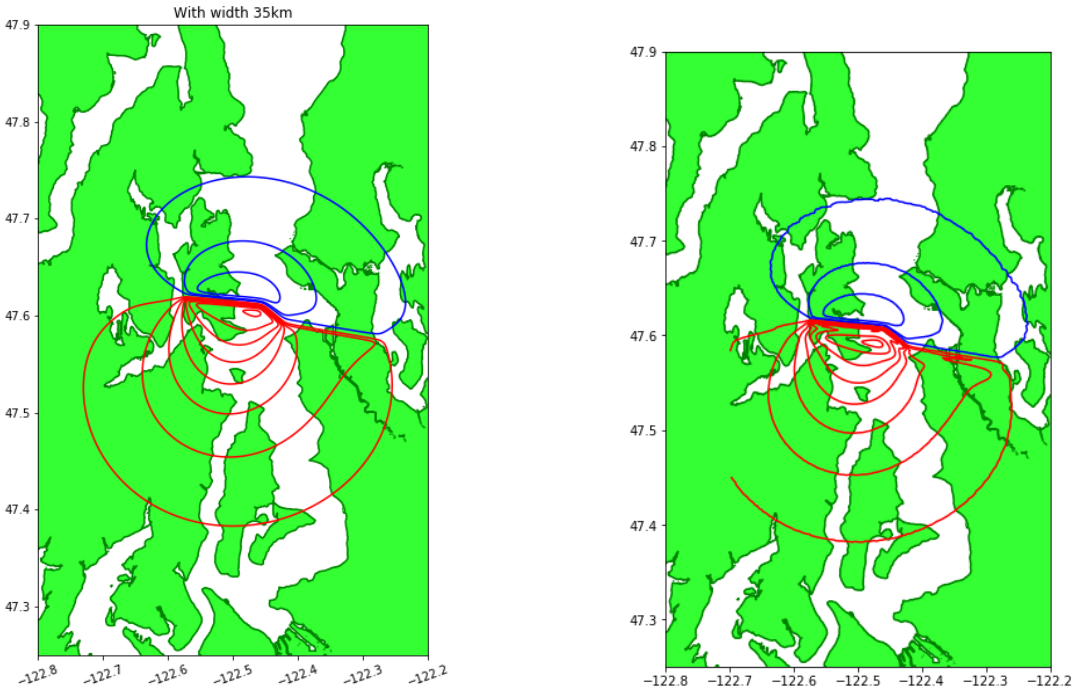

Figure 24: Left: SF-L deformation generated from subfault parameters of PMEL-124 [25], but with subfault width set to 35 km. Right: SF-L deformation provided by DNR. In both cases the red uplift contours are at increments of 1 m and the blue subsidence contours are at incrments of 0.5 m to agree with Figure 2 of [25].

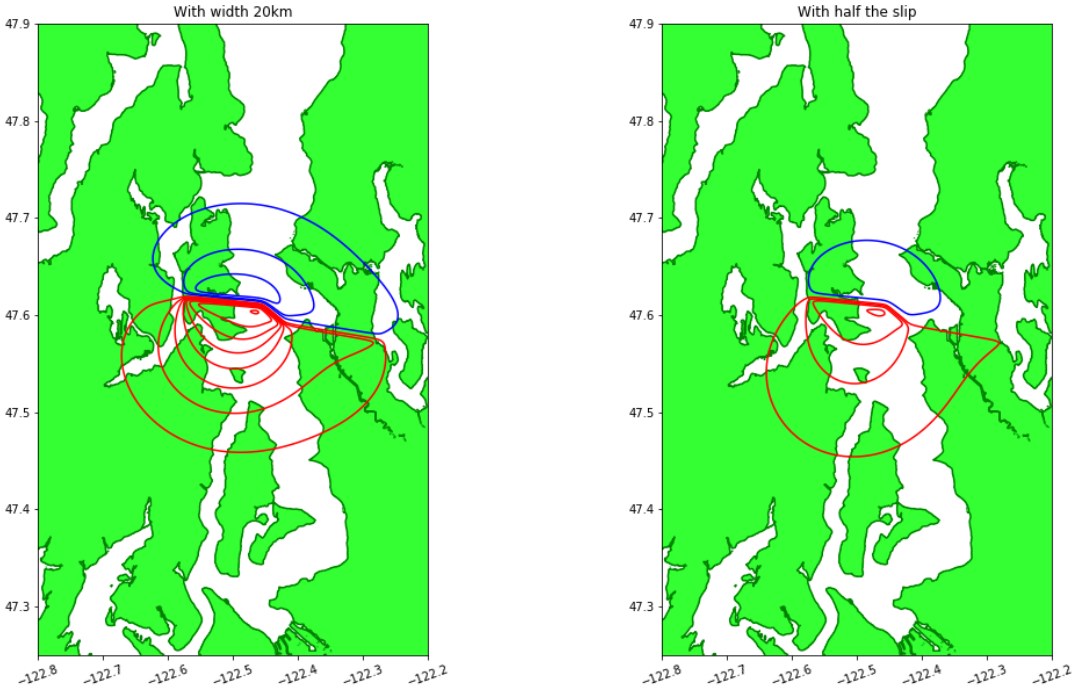

Figure 25: Left: SF-L deformation generated by setting subfault width to 20 km. Right: SF-L deformation generated by setting subfault width to 35 km but halving the slip on each subfault to recover a Mw 7.35 event.

E.2 The SF-S event

The SF-S event was used to perform some tsunami simulations in the early stages of this study. It was determined that the inundation and currents observed in Snohomish County are negligible, and so the final results provided from this study do not include SF-S simulation results.

However, in this section we collect some information about this source since several issues arose in determining the proper specification of this source based on past work. For future modeling studies where SF-S may be important, this section may prove useful.

The SF-S model was apparently first used in a PMEL study of Everett in PMEL-147 [3]. It is based on the SF-L model but is reduced to having only 4 subfaults (A2, A3, A4, and part of A5 from the SF-L subfaults of Table 3. The fault was shortened and slip values were also reduced in order to define a smaller event (claimed to be Mw 6.7) with a 50-year return time. Some of the subfault parameters are given in Table 5. The width was set to 35 km.

For reasons we do not understand, the dip was changed from 60° to 45° on all subfaults. According to Tim Walsh (personal communication), this was possibly done in order to better match observations of displacement in a trench at Vasa Park in Bellevue that might have corresponded to a Mw 6.7 type event several thousand years ago, as discussed in the EERI report [23] concerning the development of a Seattle Fault Mw 6.7 scenario. This report contains a wealth of information, but unfortunately does not give fault parameters or surface deformation in a format useful for our needs.

We also do not understand why the slip on each subfault was set to 2.8 m. According to our calculations, this gives an event with Mw 7.04, not 6.7. We find that if we instead set the slip to 1 m on each subfault, then the magnitude is Mw 6.74. Note that in the MOST input files used at PMEL the slip is set to 1 m for "unit sources" and the deformation is later scaled by the slip value. We do not know if this is related.

These parameters were taken from Table 2 of [3]. In that report there is no discussion of the depth of the subfaults, but we assume they should be the same as the SF-L scenario, where a value of 500 m (from top of fault to surface) was inferred from MOST input files provided by PMEL for SF-L.

The MOST input files provided for the SF-S event have the same parameter "htop" set to 15 km for the SF-S event. We were told that "htop" might be the distance from the *bottom* of the fault plane to the surface, but this does not make sense since with a width of 35 km and dip of 45°, the vertical distance from the top to bottom of the fault plane is $35\cos(45°) = 24$ km, and even with a dip of 60° the distance is 17.5 km, so if the bottom is at 15 km the fault would extend many km into the air. However, if the fault width were assumed to be 20 km then with dip 45° the vertical extent of the fault is 14.14 km, so setting the lower edge at 15 km would make sense. This is inconsistent with Table 2 of [3], which states the width is 35 km for each subfault.

Moreover, the plot shown in Figure 2 of [3], and the deformation files provided to us by PMEL, show a deformation that we can obtain only by placing the *top* of the fault at 15 km depth. This puts the fault much deeper than it should be and gives less surface deformation than was presumably intended. On the other hand this is counterbalanced by the increased slip and width of the fault relative to what we think was intended.

In Table 6 we present the various sets of parameters and the surface deformation at the same three locations considered using different versions of the SF-S scenario.

Figure 26 shows the surface deformation we obtain using the parameters of [3] and a depth of 15 km, and the deformation we obtain with our best guess at what the intended parameters are, which is shown in the row labelled "our best guess" of Table 6. Note that because of the cancellation of effects the maximum deformation is similar in these two plots, but the shape is very different. Moving the fault to 15 km depth gives much a more diffuse effect at the surface.

Another mystery arises when trying to reconcile the deformations we compute from the fault parameters to the deformation files provided to us by PMEL and DNR, both of which should be for this scenario but do not agree with each other or with any of the deformations we generated. PMEL provided 4 deformation files used by MOST, one for each subfault. Adding them up gives the deformation shown on the left in Figure 27. DNR provided `B_seafaultEERI/everett_b_deformation.asc` in NAD83 Washington State Plane North coordinates with horizontal units in feet (but vertical units in meters, apparently). Converting

this to WGS84 latitude-longitude coordinates gives the plot shown on the right in Figure 27. The 0.5 m contour in this plot agrees quite well with the corresponding contour in Figure 2(b) of PMEL-147 [3].

For modeling Snohomish County, the differences in these deformations makes little difference because in any case the tsunami is very small, with minimal flooding and current velocities below 1 m/s almost everywhere (see Figure 28). For the upcoming study of Bainbridge Island, it may be more important to decide on the right version of SF-S to use.

Subfault	Longitude	Latitude	Length	Strike	Slip
B1	-122.6165584	47.6157655	6.3 km	86.6°	2.8 m
B2	-122.5154909	47.6132604	8.9 km	96°	2.8 m
B3	-122.4397627	47.6000508	3.3 km	128.8°	2.8 m
B4	-122.384815	47.5868088	5.8 km	99.3°	2.8 m

Table 5: Seattle Fault SF-S. This table shows the primary parameters for the subfaults of Table 2 in [3]. A width of 35 km and dip of 45° has been used for all subfaults in [3]. The longitude and latitude is for the top center of the subfault, and has been inferred from the literature. Note that B1–B3 correspond to A2–A4 of Table 3 while B4 is a shortened version of A5, with the top center coordinates adjusted accordingly.

Source	Model parameters					Deformation			
	Width	Dip	Depth	Slip	Magnitude	Alki Pt.	Rest. Pt.	West Pt.	Max
PMEL-147 [3]	35	45	15	2.8	7.2	0.61	0.67	0.28	0.72
w/modified depth	35	45	0.5	2.8	7.2	1.47	1.85	−0.14	2.03
+modified width	20	45	0.5	2.8	7.04	1.39	1.76	−0.13	1.99
Our best guess	20	60	0.5	1.0	6.74	0.52	0.61	-0.10	0.70
MOST Deform.	?	?	?	?	?	0.21	0.23	0.20	0.24
DNR Deform.	?	?	?	?	?	0.59	0.65	0.55	0.68

Table 6: Seattle Fault SF-S. This table shows the observed uplift or subsidence (deformation) at three locations, as well as the maximum uplift. The first three rows show the original values from PMEL-147, with the depth moved to 0.5 km, and with the width also reduced from 35 to 20 km. "Our best guess" is the values we think were originally intended. The MOST deformation file was provided by PMEL and the DNR deformation file was provided by DNR, both supposedly were what was used in the PMEL-147 study.

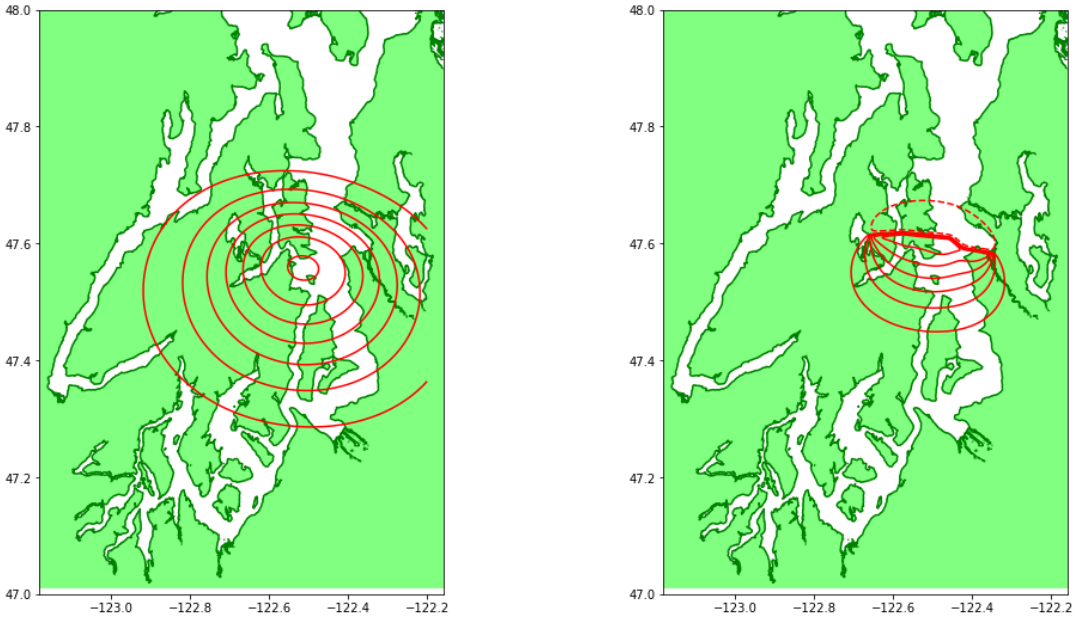

Figure 26: Left: Deformation generated with fault parameters specified in PMEL-147 [3] and with the depth set to 15 km at the top of the fault. Maximum uplift is 0.72 m. Right: Deformation generated with our best guess at the intended fault parameters, the row in Table 6 labelled "our best guess". Maximum uplift is 0.70 m. In both cases the contours are at increments of 0.1 m.

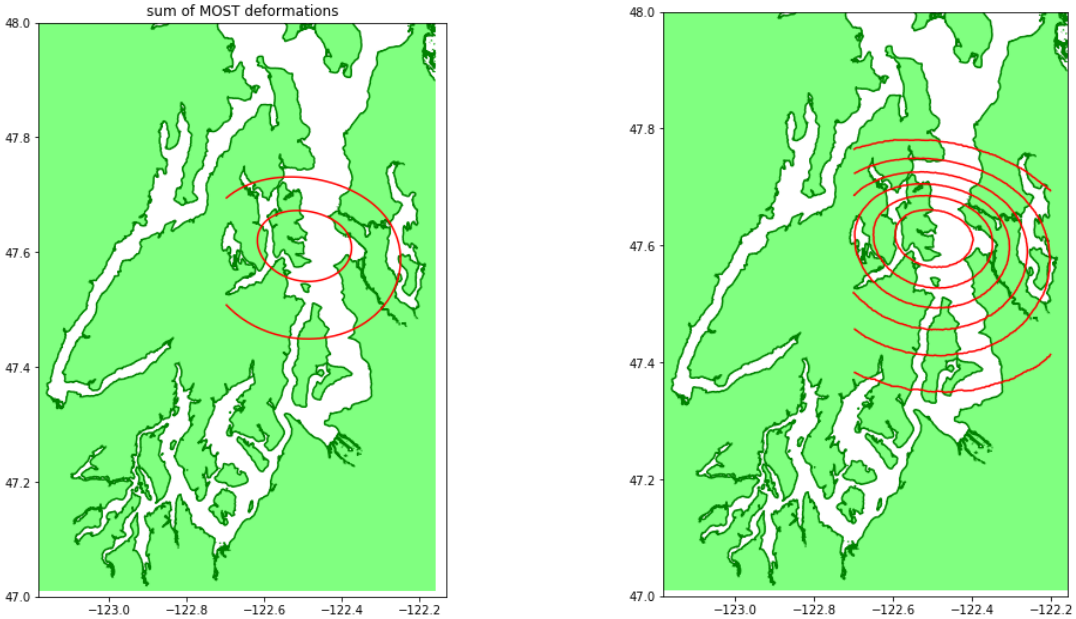

Figure 27: Left: Deformation provided by PMEL from MOST input files. Maximum uplift is 0.24 m. Right: Deformation provided by DNR as `B_seafaultEERI`. Maximum uplift is 0.68 m. In both cases the contours are at increments of 0.1 m.

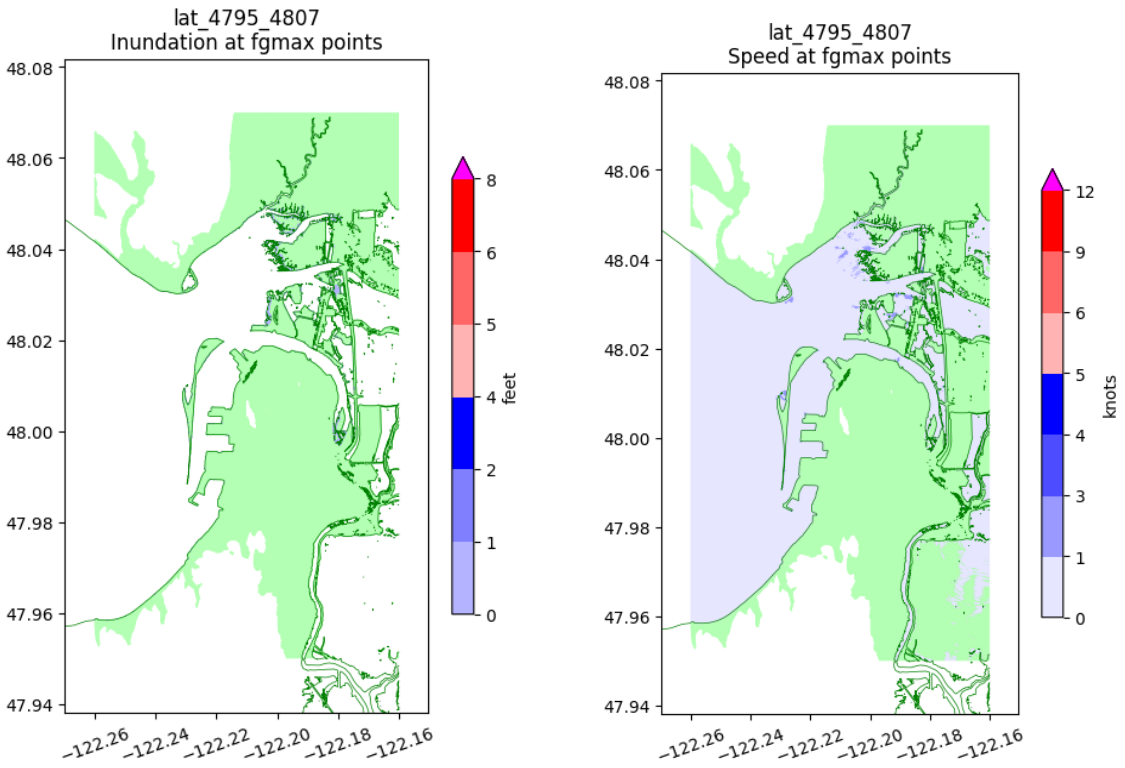

Figure 28: Maximum flow depth (left) and speed (right) calculated near Everett using our best guess at the proper SF-S model. Compare to Figure 16, which shows results with the SF-L model.

Acknowledgments

The earthquake deformation files for the CSZ L1 and SF-L events were provided by PMEL. Many thanks to Kelly Carignan at NCEI for rapidly developing the merged DEM discussed in Section 3.

References

[1] B. Atwater, M.-R. Satoko, K. Satake, T. Yoshinobu, U. Kazue, and D. Yamaguchi. USGS professional paper 1707, 2005.

[2] M. J. Berger, D. L. George, R. J. LeVeque, and K. T. Mandli, *The geoclaw software for depth-averaged flows with adaptive refinement.* Preprint and simulations: www.clawpack.org/links/papers/awr10, 2010.

[3] C. Chamberlain and D. Arcas, *Modeling tsunami inundation for hazard mapping at Everett, Washington, from the Seattle Fault.* OAA Technical Memorandum OAR PMEL-147, 2015, https://doi.org/10.7289/V59Z92V0, https://repository.library.noaa.gov/view/noaa/11189.

[4] Clawpack Development Team, *Clawpack software*, 2017, https://doi.org/10.5281/zenodo.820730, http://www.clawpack.org. Version 5.4.1.

[5] ESRI, *ESRI ASCII Raster format.* http://resources.esri.com/help/9.3/arcgisdesktop/com/gp_toolref/spatial_analyst_tools/esri_ascii_raster_format.htm, Accessed 2018.

[6] A. D. Frankel, M. D. Petersen, C. S. Mueller, K. M. Haller, R. L. Wheeler, E. V. Leyendecker, R. L. Wesson, et al., *Documentation for the 2002 update of the national seismic hazard maps.* U.S. Geological Survey Open-File Report 02-420, 2002, http://geohazards.cr.usgs.gov/eq/of02-420/OFR02-420.pdf.

[7] A. D. Frankel, W. J. Stephenson, D. L. Carver, et al., *Seismic Hazard Maps for Seattle, Washington, Incorporating 3D Sedimentary Basin Effects, Nonlinear Site Response, and Rupture Directivity.* ?, 2007.

[8] C. Garrison-Laney, *A comparison of L1 and similar Cascadia earthquake sources used in Washington State tsunami modeling.* Available on request, 2017.

[9] F. González, R. J. LeVeque, J. Varkovitzky, P. Chamberlain, B. Hirai, and D. L. George, *GeoClaw Results for the NTHMP Tsunami Benchmark Problems.* http://depts.washington.edu/clawpack/links/nthmp-benchmarks/geoclaw-results.pdf, 2011.

[10] F. González, B. Sherrod, B. Atwater, A. Frankel, S. Palmer, et al., *2002 Puget Sound Tsunami Sources Workshop Report. A contribution to the Inundation Mapping Project of the U.S. National Tsunami Hazard Mitigation Program.* NOAA OAR Special Report, 2003.

[11] S. Y. Johnson, S. V. Dadisman, J. R. Childs, and W. D. Stanley, *Active tectonics of the seattle fault and central puget sound, washingtonimplications for earthquake hazards*, Geol. Soc. Amer. Bull., 111 (1999), pp. 1042–1053, https://doi.org/10.1130/0016-7606.

[12] S. Koshimura, H. O. Mofjeld, F. I. González, and A. L. Moore, *Modeling the 1100 bp paleotsunami in Puget Sound, Washington*, Geophysical Research Letters, 29 (2002), p. 1948, https://doi.org/10.1029/2002GL015170, http://onlinelibrary.wiley.com/doi/10.1029/2002GL015170/abstract.

[13] S. Koshimura, A. L. Moore, and H. O. Mofjeld, *Simulation of paleotsunamis in Puget Sound, Washington*, in International Tsunami Symposium 2001 Proceedings, ?, ed., vol. ? of ?, ?, 2001, pp. 761–773.

[14] R. J. LeVeque, D. L. George, and M. J. Berger, *Tsunami modeling with adaptively refined finite volume methods*, Acta Numerica, (2011), pp. 211–289.

[15] R. J. LeVeque, F. I. González, and L. M. Adams, *Tsunami Hazard Assessment of Snohomish County, Washington.* (website containing reports and data), 2018, http://depts.washington.edu/ptha/WA_EMD_Snohomish/.

[16] NCEI, *Port Townsend 1/3 Arc-second MHW Coastal Digital Elevation Model.* https://www.ngdc.noaa.gov/metaview/page?xml=NOAA/NESDIS/NGDC/MGG/DEM/iso/xml/366.xml&view=getDataView&header=none, Accessed 2017.

[17] NCEI, *Puget Sound 1/3 Arc-second MHW Coastal Digital Elevation Model.* https://www.ngdc.noaa.gov/metaview/page?xml=NOAA/NESDIS/NGDC/MGG/DEM/iso/xml/5164.xml&view=getDataView&header=none, Accessed 2017.

[18] NCEI, *Strait of Juan de Fuca 1/3 arc-second NAVD 88 Coastal Digital Elevation Model.* https://www.ngdc.noaa.gov/metaview/page?xml=NOAA/NESDIS/NGDC/MGG/DEM/iso/xml/11514.xml&view=getDataView&header=none, Accessed 2017.

[19] NGDC, *Registration of structured square-cell grids.* https://www.ngdc.noaa.gov/mgg/global/gridregistration.html, Accessed 2018.

[20] M. D. Petersen, C. H. Cramer, and A. D. Frankel, *Simulations of Seismic Hazard for the Pacific Northwest of the United States from Earthquakes Associated with the Cascadia Subduction Zone*, Pure Appl. Geophys., 159 (2002), pp. 2147–2168.

[21] T. L. Pratt, S. Johnson, C. Potter, W. Stephenson, and C. Finn, *Seismic reflection images beneath Puget Sound, western Washington State: The Puget Lowland thrust sheet hypothesis*, Journal of Geophysical Research: Solid Earth, 102 (1997), pp. 27469–27489, https://doi.org/10.1029/97JB01830, http://onlinelibrary.wiley.com/doi/10.1029/97JB01830/abstract.

[22] K. Satake, K. Wang, and B. F. Atwater, *Fault slip and seismic moment of the 1700 Cascadia earthquake inferred from Japanese tsunami descriptions*, J. Geophys. Res., 108(B11) (2003), p. 2535, https://doi.org/10.1029/2003JB002521.

[23] M. Stewart et al., *Scenario for a Magnitude 6.7 Earthquake on the Seattle Fault.* Earthquake Engineering Research Institute and Washington Military Department, Emergency Management Division, 2015, https://www.eeri.org/projects/earthquake-scenarios/seattle-fault-scenario/.

[24] U. S. ten Brink, P. C. Molzer, M. A. Fisher, et al., *Subsurface geometry and evolution of the Seattle fault zone and the Seattle basin, Washington*, Bull. Seismol. Soc. Am., 92 (2002), pp. 1737–1753.

[25] V. V. Titov, F. I. González, H. O. Mofjeld, and A. J. Venturato, *NOAA TIME Seattle tsunami mapping project: procedures, data sources, and products.* NOAA Technical Memorandum OAR PMEL-124, 2003, https://repository.library.noaa.gov/view/noaa/11033.

[26] A. J. Venturato, D. Arcas, V. V. Titov, H. O. Mofjeld, C. C. Chamberlain, and F. I. González, *Modeling tsunami inundation for hazard mapping at Everett, Washington, from the Seattle Fault.* NOAA Technical Memorandum OAR PMEL-132, 2007, https://repository.library.noaa.gov/view/noaa/11070.

[27] Washington State EMD, *Modeling a Magnitude 7.4 Earthquake on the Southern Whidbey Island Fault Zone.* https://mil.wa.gov/uploads/pdf/seismic-safety-committee/whidbey%20island%20fault%20zone.pdf, Accessed 2018.

[28] Wikipedia, *Puget sound faults.* https://en.wikipedia.org/wiki/Puget_Sound_faults, 2018.

[29] Wikipedia, *Esri grid.* https://en.wikipedia.org/wiki/Esri_grid, Accessed 2018.

[30] R. C. Witter, Y. Zhang, K. Wang, G. Priest, C. Goldfinger, L. Stimely, J. English, and P. Ferro, *Simulating tsunami inundation for a range of Cascadia megathrust earthquake scenarios at Bandon, Oregon USA*, Geosphere, 9 (2013), pp. 1783–1803.